

Spatio-temporal patterns and drivers of terrestrial Dissolved Organic Carbon (DOC) leaching to the European river network.

Céline Gommet^{1,3}, Ronny Lauerwald², Philippe Ciais³, Bertrand Guenet⁴, Haicheng Zhang¹, Pierre Regnier¹

¹Biogeochemistry and Earth System Modelling, Department of Geoscience, Environment and Society, Université Libre de Bruxelles, Bruxelles, Belgium

²Université Paris-Saclay, INRAE, AgroParisTech, UMR ECOSYS, 78850, Thiverval-Grignon, France

³Laboratoire des Sciences du Climat et de l'Environnement, UMR8212, CEA-CNRS-UVSQ F-91191 Gif sur Yvette, France

⁴Laboratoire de Géologie, UMR 8538, Ecole Normale Supérieure, IPSL, PSL Research University, CNRS, Paris, France

Correspondence to: Céline Gommet (celine.gommet@ulb.be)

Abstract. Leaching of dissolved organic carbon (DOC) from soils to the river network is an important component of the land carbon (C) budget. At regional to global scales, its significance has been estimated through simple mass budgets, often using multi-year averages of observed fluvial DOC fluxes as proxy of DOC leaching due to the limited availability of observations of the leaching flux itself. This procedure leads to a systematic underestimation of the leaching flux because of the decay of DOC during fluvial transport. Moreover, this procedure does not allow revealing spatio-temporal variability in DOC leaching from soils, which is vital to better understand the drivers of DOC leaching and its impact on the local soil C budget. In this study, we use the land surface model ORCHILEAK to simulate the terrestrial C budget including leaching of DOC from the soil and its subsequent reactive transport through the river network of Europe. The model performance is evaluated not only against the sparse observations of soil DOC leaching rate, but also against the more abundant observations of fluxes and reactivity of DOC in rivers, providing further evidence that our simulated DOC fluxes are realistic. The model is then used to simulate the spatio-temporal patterns of DOC leaching across Europe over the period 1972–2012, quantifying both the environmental drivers of these patterns as well as the impact of DOC leaching on the land C budget. Over the simulation period, we find that, on average, 14.3 TgC yr⁻¹ of DOC is leached from land to European rivers, which is about 0.6% of the terrestrial net primary production, a fraction significantly lower than that reported for tropical river networks. On average, 12.3 TgC yr⁻¹ of the leached DOC is finally exported to the coast via the river network, and the rest is respired during transit. DOC leaching presents a large seasonal variability, with the maximum occurring in winter and the minimum in summer, except for most part of the Northern Europe where the maximum occurs in spring due to the snow melt. DOC leaching rate is generally low in warm and dry regions, and high in cold and wet regions of Europe. Furthermore, runoff, and the ratio between runoff from shallower flow paths vs. deep drainage and groundwater flow, are the main drivers of the spatio-temporal variation of DOC leaching. Temperature, as a major control of DOC production and decomposition rates in the soils, plays only a secondary role.

38 **1 Introduction**

39 Terrestrial ecosystems are an important carbon (C) sink as they absorb about one fourth of anthropogenic CO₂
40 emissions and store these C in plant biomass and soil carbon pools (Friedlingstein et al., 2020). This terrestrial C
41 sink mitigates the growth rate of atmospheric CO₂ concentration and thus plays an important role in regulating
42 climate change (Ciais et al., 2013). However, the efficiency of that sink is partly alleviated by the permanent,
43 lateral leaching of C from soils, through the river network down to the ocean (Regnier et al., 2013). An accurate
44 understanding of lateral C fluxes through the river network is thus necessary to better understand the global C
45 cycling and to inform policies of climate change mitigation (Le Quéré et al., 2018).

46 The identification of riverine C transfers as a key component of the continental C budget constituted an
47 important paradigm shift in our understanding of the global C cycle (Cole et al., 2007). More recently, riverine C
48 cycling was also shown to be affected by anthropogenic perturbation and thus to be an element of the
49 anthropogenic CO₂ budget (Regnier et al., 2013; Le Quéré et al. 2015). Anthropogenic perturbations of riverine
50 C fluxes are manifold and comprise direct impacts through changing C and nutrient inputs following land-use
51 change and agricultural activities, wastewater discharge, and hydraulic management (e.g. Tian et al., 2015;
52 Lauerwald et al., 2020; Hastie et al., 2021; Maavara et al., 2017). There are also indirect impacts following
53 climate change and changes in atmospheric composition. Together, these perturbations have accelerated the
54 turnover of C along the terrestrial-inland water continuum. The terrestrial C sink, which is classically estimated
55 without taking into account the C exports through the river network, is thus generally overestimated (Regnier et
56 al., 2013; Lauerwald et al., 2020).

57 The integration of riverine C transfers into the terrestrial C budget requires the quantification of the amount of C
58 lost from soils to the river network. Due to the scarcity of observational data, this flux is not easy to estimate
59 based on empirical methods. At global scale, this flux was constrained through budget closure based on
60 estimates of riverine C exports to the coast, and estimates of C losses to the atmosphere and aquatic sediments
61 during transport. The existing global estimates of these soil C exports to the river network, as synthesized by
62 Drake et al. (2018), range from 1.1 to 5.1 PgC yr⁻¹ – a huge uncertainty range reflecting the limitations of
63 empirical estimation approaches and the paucity of underlying data. Over the past decade, a new generation of
64 land surface models (LSMs) have been developed, which represent the export of C from soils to the river
65 network, and in some cases even the transport and cycling of these terrestrial C loads along the river network
66 down to the coast (Smith et al. 2010; Kicklighter et al. 2013; Tian et al., 2015; Lauerwald et al., 2017; Nakhavali
67 et al., 2018). With the exception of the study by Tian et al. (2015), all these studies focus on the lateral export of
68 dissolved organic C (DOC) which is a product of the incomplete decomposition of plant litter and soil organic
69 carbon (SOC). These mechanistically based models allow to predict the leaching of DOC in unmonitored regions
70 and to assess the spatial and temporal variability which, to date, can only be poorly resolved by empirical
71 methods. Moreover, these approaches link the C exports from soils to the river network to the terrestrial C cycle,
72 and thus allow to directly assess the role of these C exports on the terrestrial C budget, its perturbation through
73 changes in land use, climate and atmospheric chemistry, and its impact on the terrestrial sink for anthropogenic
74 CO₂ emissions.

75 In this study, we use the LSM ORCHILEAK (Lauerwald et al. 2017), a branch of the IPSL-LSCE LSM
76 ORCHIDEE (Krinner et al. 2005), to quantify the DOC leaching from soils and its effects on the terrestrial C
77 budget in Europe. ORCHILEAK not only simulates the vertical C cycling between vegetation, soils and
78 atmosphere in response to climate, atmospheric CO₂ concentrations, and land use change, but also represents the
79 lateral exports of DOC from soils to the river network as well as the reactive transport of that DOC through the
80 river network. To our knowledge, only one study (Kindler et al., 2011) has estimated the soil DOC leaching flux
81 based on runoff and direct observations of DOC concentrations in the soil water for various locations across
82 Europe. Thus, this empirical assessment will be used for evaluating the simulated DOC leaching fluxes in this
83 study. Further, we evaluate simulated against observed riverine DOC fluxes, which are obtained from different
84 water quality surveys and scientific publications. Assuming a realistic representation of DOC reactivity in the
85 river network, which is to be evaluated against observations as well, this model-data comparison of riverine
86 DOC fluxes represents a valuable and additional possibility to assess the validity of simulated soil DOC
87 leaching.

88 So far, ORCHILEAK has been successfully tested and applied on large, near-natural river systems such as the
89 Amazon (Lauerwald et al. 2017, Hastie et al. 2019, Lauerwald et al. 2020), the Congo (Hastie et al. 2021) and
90 the Lena Rivers with a version also including some specific permafrost related mechanisms (Bowring et al.
91 2019, 2020). In this study, for the first time, ORCHILEAK is applied to, and evaluated for, the European river
92 network which is subject to direct impacts of agricultural land use, in contrast to more natural river basins. For
93 this reason, we devote special attention to manure application as an anthropogenic non-point source of DOC to
94 the river network, while we assume that for the period of simulation (1979-2012), due to the quality of sewage
95 water treatment, anthropogenic point sources of DOC are now negligible for most parts of Europe. Moreover, as
96 shown for instance by Meybeck (1986), DOC from sewage is highly labile and only affects concentration within
97 short distances downstream of water processing plants. Avoiding observational data from sites that are known to
98 be directly impacted by sewage inputs, we are able to evaluate model performance with regard to fluvial
99 transfers of soil derived DOC, which is the focus of our study.

100 Making full use of the capabilities of the ORCHILEAK model, we study in detail the spatio-temporal patterns in
101 DOC leaching and its quantitative contribution to the terrestrial C budget across Europe. We investigate how
102 specific climate zones in Europe differ with regard to seasonality in DOC leaching fluxes, which are
103 hypothesized to be controlled by hydrology, litter fall and temperature effects on litter and SOC decomposition.
104 We will further try to quantify the effect of these controls in the different climate zones of Europe. Finally, we
105 strive to find out in which climate zone DOC leaching affects the terrestrial C budget the most.

106 **2 Methodology**

107 **2.1 ORCHILEAK**

108 **2.1.1 Model overview**

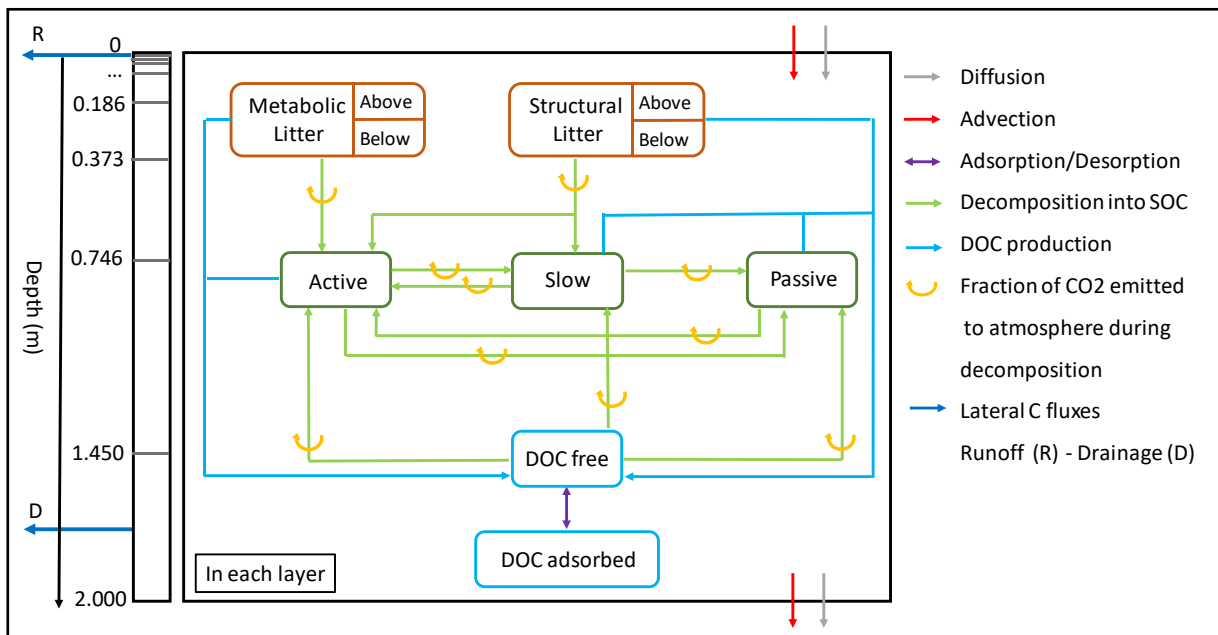
109 ORCHILEAK (Lauerwald et al., 2017) is a branch of the model ORCHIDEE (Organizing Carbon and
110 Hydrology in Dynamic Ecosystems) (Krinner et al., 2005), the land surface component of the Institut Pierre-
111 Simon Laplace (IPSL) Earth system model (ESM). ORCHIDEE simulates energy, water and C fluxes between
112 the atmosphere and the land at a global scale. This LSM is based on four sub-modules. The first one, SECHIBA,
113 simulates the energy budget (energy, carbon and water) between the atmosphere and the biosphere as well as the
114 hydrology, which in the default set-up used here, are both represented using a 30 minute time-step. The second
115 sub-module, adapted from the LPJ model (Sitch et al., 2003), represents the dynamics of vegetation distribution
116 on long time scales (1 year), while the third one (STOMATE) simulates the C dynamics in vegetation and soils
117 at a daily to sub-daily step (Krinner et al., 2005). Finally, the fourth sub-module handles the routing of water that
118 is lost via surface runoff and drainage from soils to the ocean through the global river network (Polcher 2003,
119 Guimberteau et al., 2012), for which a daily time-step is used. All processes are simulated on a horizontal model
120 grid, the resolution of which can be adapted to that of the meteorological forcing files. In this study, simulations
121 are run at a spatial resolution of 0.5°. Moreover, in the default set-up, up to 13 plant function types (PFTs; bare
122 soil, eight types of forest, two types of grassland and two types of cropland) can be distinguished for each cell,
123 for which C budgets are simulated individually, while energy and water budgets are simulated at the grid cell
124 level.

125 ORCHIDEE represents the soil C dynamics distinguishing different pools of plant litter and soil organic C over a
126 2 m profile. A branch of ORCHIDEE, called ORCHIDEE-SOM (Camino et al. 2018), added a vertical
127 discretization of these carbon pools over 11 layers and included the representation of DOC production and
128 cycling within the soil column (see section 2.1.2 for more details). ORCHILEAK was built on this branch and
129 accounts for the coupled reactive transport processes impacting the dissolved C inputs from soils to the river
130 network, including both DOC leaching from soils and CO₂ produced by soil respiration, into the hydrologic
131 routing scheme. Besides advective transport of carbon with the water flow, ORCHILEAK simulates the
132 decomposition of DOC during riverine transport, the gas exchange of CO₂ at the interface between the inland
133 water and the atmosphere, and the exchange of C between water column and soil column in inundated
134 floodplains. For the representation of in-river DOC decomposition, two pools with different decay rates are
135 distinguished, a slow (refractory DOC) and a fast (labile DOC) pool. All those fluxes are closely coupled to the
136 model representation of hydrology that comprises interception of precipitation, throughfall, infiltration,
137 percolation, surface runoff, drainage, and the routing of discharge along the river-floodplain network.

138

139 **2.1.2 Soil carbon module**

140 The soil carbon module of ORCHILEAK (Fig. 1) is derived from the CENTURY soil carbon model of Parton et
 141 al. (1988). In the standard scheme (Krinner et al., 2005), C in the soil of each model grid cell, and for each PFT,
 142 is represented by four different litter and three different soil organic carbon (SOC) pools with different turnover
 143 rates. The four litter pools correspond to metabolic aboveground and belowground litter, structural aboveground
 144 and belowground litter (Fig. 1). The SOC is subdivided into active, slow and passive pools, which have different
 145 default decomposition rates that are further modified at each time-step according to the evolving soil moisture
 146 and soil temperature. In the CENTURY scheme, C from the decomposed structural litter enters the active and the
 147 slow pools with the fraction allocated to each pools depending on lignin content of the litter, while the entire
 148 metabolic litter pool and the remaining part of structural litter is allocated to the active SOC pool. The SOC
 149 pools then feed into each other with the main C flux going from active to slow and passive to represent microbial
 150 decomposition of detrital organic matter, and a small return flux of slow and passive C back to the active pool to
 151 represent implicitly the C supply in the form of dead microbial biomass.



152
 153
 154 **Figure 1. The new version of the soil module of ORCHILEAK-SOM. The left box represents the discretization of the**
 155 **soil column and the transport processes between layers. The right box is a zoom of all the biogeochemical**
 156 **transformation processes that occur in each layer.**

157
 158 Camino et al. (2018) updated this scheme with a vertical discretization of distinct SOC and litter pools over a 2
 159 m soil profile represented by 11 layers, with geometrically increasing thickness from top to bottom (Figure 1).
 160 Camino et al. (2018) further developed the soil C module by including an explicit representation of the fate of
 161 DOC along this vertically discretized soil profile. Processes accounted for are DOC production from the
 162 decomposition of SOC and litter, decomposition of DOC within the soil, sorption/desorption of DOC onto/from
 163 mineral surfaces, vertical advection and diffusion of DOC through the soil column, and lateral, advective

164 leaching of DOC out of the soil profile, along with surface runoff (water flux from the topsoil surface) and
 165 drainage (water flux from the last layer soil at 2m depth). In each soil layer, ORCHILEAK explicitly simulates
 166 the fresh litter input (depending on the simulated vertical root distribution), decomposition of each organic
 167 matter pool (including litter and SOC), C transformation between different organic matter pools (showed by blue
 168 and green arrows between different pools in Fig. 1), C transport and diffusion between neighboring soil layers,
 169 and the loss of DOC due to leaching. For a specific organic C pool at each time step, only a fraction of the
 170 decayed C is respired as CO₂ to the atmosphere (orange arrows in Fig. 1), the remaining being transferred to
 171 other organic pools (to mimic microbial growth and mortality).

172 The DOC dynamics in the soil is simulated according to equation (1), which accounts for the dynamic interplay
 173 between production, decomposition, transport and sorption-/desorption processes along the discretized 2 m soil
 174 column. All processes are simulated using a 30-minute time-step in following order: Firstly, production and
 175 decomposition of DOC are calculated, and DOC stocks for each layer and pool are updated accordingly.
 176 Secondly, vertical exchange of DOC between soil layers is simulated in two steps, first for the process of DOC
 177 advection with the flow of water through the soil column, then for diffusion of DOC. Lastly, the export of DOC
 178 through leaching from top- and bottom soil with runoff and drainage, respectively, are calculated.

179

$$\frac{dDOC_i}{dt} = \sum (Production_i - Decomposition_i) + F_{A,i} + F_{D,i} \quad (1)$$

180 In equation (1), i stands for the index of each layer. Each layer is connected to the adjacent layers by advective
 181 (F_A) and diffusive (F_D) fluxes. The total DOC transport flux is made of an advective component (equation 2)
 182 computed as the product of the water flux Q and the concentration of free DOC in the water solution of the i^{th}
 183 layer and a diffusive component that follows Fick's first law (equation 3):

$$F_A = Q * DOC_i \quad (2)$$

$$F_D = -D * \frac{\partial^2 DOC}{\partial z^2} \quad (3)$$

184 where i stands for the i th layer, z is the depth along the discretized soil profile, and D stands for the molecular
 185 diffusion coefficient of DOC, which is assigned a value of $1.06 \times 10^{-5} \text{ m}^2 \text{ d}^{-1}$ (Ota et al., 2013).

186 The advective export of DOC to the river network is proportional to the top (first five layers, 4.5 cm) and bottom
 187 (11th layer) DOC concentrations, corresponding to water loss fluxes associated to runoff (for near surface) and
 188 drainage (for deep soil layer). Diffusion of DOC between adjacent soil layers is proportional to the gradient in
 189 DOC concentrations in the soil solution (eq. 3), moving towards an equilibrium. In addition, we apply a Fickian-
 190 type transport to represent the effect of bioturbation on SOC profiles. In this case, the transport is represented

191 similar to eq. 3, but follows the gradient in SOC concentration relative to the volume of the soil layer.
 192 Representing bioturbation as a diffusion-like process is a common approach in LSMs with vertically discretized
 193 SOC scheme (Camino et al., 2018). However, bioturbation is much slower than diffusion of DOC in the soil
 194 solution, with a diffusion coefficient $D = 2.74 \times 10^{-7} \text{ m}^2 \text{ d}^{-1}$ (Koven et al. 2013), compared to $D = 1.06 \times 10^{-5} \text{ m}^2 \text{ d}^{-1}$
 195 (Ota et al., 2013). Therefore, bioturbation impacts the vertical SOC profile while it has only a marginal influence
 196 on the DOC dynamics. The right hand-side of Fig. 1 summarizes the set of production/decomposition processes
 197 that occur in each layer. During litter decomposition, a fraction of the C is directly emitted back to the
 198 atmosphere as CO_2 while the remainder feeds the active and slow SOC pools:
 199

$$CO_2 \text{ respiration}(Litter) = (1 - CUE) * k_L * (1 - \omega_L) * Litter \quad (4)$$

$$Litter \text{ decomposition} = CUE * k_L * (1 - \omega_L) * Litter \quad (5)$$

200 where k_L is the kinetic rate for the litter decomposition (dependent on soil moisture and temperature (Camino et
 201 al., 2018)) and ω_L the fraction of litter that is channelled into DOC production (as opposed to particulate SOC).
 202 This approach of relating DOC production directly to the decomposing litter is inspired by Nakhavali et al.
 203 (2018) (following the ECOSSE model (Smith et al., 2010)) and is a major modification compared to the
 204 previous version of soil DOC and POC cycling from Camino et al., 2018. In Eqs. (4) and (5), the partitioning
 205 between SOC production and respiration is defined by the carbon use efficiency (CUE).
 206 In turn, active SOC is degraded into both slow and passive SOC and the respiration fluxes associated with these
 207 processes are also controlled by the CUE (Eqs. 6 and 7, with k_{SOC} as the kinetic rate for SOC decomposition,
 208 which depends on soil moisture and soil temperature, and ω_{SOC} as the fraction of decomposed SOC that is
 209 transformed into DOC):
 210

$$CO_2 \text{ respiration}(SOC) = (1 - CUE) * k_{SOC} * (1 - \omega_{SOC}) * SOC \quad (6)$$

$$SOC \text{ decomposition} = CUE * k_{SOC} * (1 - \omega_{SOC}) * SOC \quad (7)$$

211
 212 The decomposition of the litter and SOC pools produces a small amount of DOC according to equation 8. The
 213 DOC pool is thus fed by seven contributing sources, one for each of the four decomposing litter pools and three
 214 from the decomposing SOC pools:
 215

$$DOC \text{ production} = k_L * \omega_L * Litter + k_{SOC} * \omega_{SOC} * SOC \quad (8)$$

216 In ORCHIDEE-SOM (Camino et al. 2018), all decomposed litter and SOC which is not respired as CO_2 , was
 217 first fed into the DOC pools, and only upon the decomposition of that DOC, the non-respired fraction of the
 218 decomposed DOC could feed the other SOC pools. Such formulation is in contrast to the adaption of the RothC
 219 SOC model in ECOSSE (Smith et al., 2010) and JULES (Nakhavali et al., 2018) that we followed here, where

220 the major exchange of C is between the different litter and SOC pools, and the production of DOC is related to
 221 these SOC and litter pools by empirical rate constants, which were fitted to reproduce observed DOC turnover
 222 times (Kalbitz et al., 2003, Turgeon, 2008) and DOC concentrations in the soil. The much higher DOC
 223 production rates simulated by ORCHIDEE-SOM in its original configuration during preliminary tests over
 224 Europe led us to implement the new approach (equations 4-7). While preserving the basic structure of
 225 ORCHIDEE-SOM, we thus adapted the model in a way that organic C exchange occurs mainly among the
 226 particulate litter and SOC pools, similar to the original Century model, while preserving the basic structure of
 227 ORCHIDEE-SOM. The production of DOC is represented as a side product of this C exchange between pools of
 228 litter and SOC, with production rates as used in ECOSSE. In the modified soil carbon module, we used the
 229 parameter ω (Eqs. 4-7) as a scaling factor that determines how much DOC is produced by the decomposition of
 230 litter and SOC. This parameter was calculated after Smith et al. (2010) as the ratio of production of DOC from
 231 litter (p_{DOC_L}) and the SOC pools ($p_{DOC_{SOC}}$) to the decomposition rates of litter (k_L) and SOC (k_{SOC}). The initial
 232 values for ω were 0.5 % and 3 % for the litter and SOC pools, respectively. Further optimization with regard to
 233 reproducing observed soil DOC concentrations led to ω values set at 0.2% for the litter and 1.2% for the SOC
 234 pools.

235 Once produced, the free DOC can then be adsorbed to soil mineral particles, and the adsorbed DOC can again be
 236 desorbed and return to the free DOC pool following a linear adsorption isotherm as described in Neff and Asner
 237 (2001) and Wu et al. (2014). We assume that equilibrium between the dissolved and adsorbed phases is
 238 instantaneous. Moreover, the work by Kothawala et al. (2008) showed that this approach performed fairly well
 239 compared to the more complex approach of using Langmuir equations. The partitioning is controlled by K_D , the
 240 so-called equilibrium partition coefficient (eq. 9), considered constant at 8.05×10^{-5} m³ water kg⁻¹ soil (Moor et
 241 al., 1992). All constants used are listed in table S1.

242

$$DOC_{adsorption-desorption\ eq} = K_D * DOC \quad (9)$$

243 Finally, the DOC pool is subject to decomposition according to equation (10) and then partly feeds into the SOC
 244 pools (eq. 11), where k_{DOC} is the DOC decay rate, which also depends on soil moisture and soil temperature.

245

$$CO_2\ respiration(DOC) = (1 - CUE) * k_{DOC} * DOC \quad (10)$$

$$SOC\ production\ by\ DOC = CUE * k_{DOC} * DOC \quad (11)$$

246 **2.1.3 Manure as an additional C source**

247 In Europe, a large fraction of the landscape is dominated by agricultural and grazing activities, and manure
 248 application represents a significant additional C - in particular DOC- source to the soil in regions dominated by
 249 grasslands and croplands. Studies have shown an increase in riverine DOC concentration related to manure
 250 application, with frequency and intensity of storm events in spring directly after manure application exerting an

251 important control on the amounts of additional DOC leached to the river network (e.g., Royer et al., 2007; Delpla
252 et al., 2011; Singh et al., 2014; Humbert et al., 2020). The type of manure input can be very different from one
253 region to another, and the physicochemical properties (e.g. C:N ratio and the ratio of dissolved and particulate
254 organic matter) depend strongly on the specific type of manure input. However, current forcing data only
255 provide the amount of total manure inputs, without information regarding specific composition and/or
256 physicochemical properties of the manure. To constrain the C flux from manure infiltrating into the soil, we used
257 the gridded estimates of manure nitrogen (manure-N) applications produced by Zhang et al. (2017) as forcing
258 file. Following the use of that data as forcing in the model branch ORCHIDEE-CNP developed by Sun et al.
259 (2021), we assumed that 90% of the total manure-N is in mineral form (i.e. NH_4^+ or NO_3^-) and the remaining
260 10% is in organic form. To convert the organic manure-N into a manure-C flux, a C:N stoichiometric ratio of
261 13.7 was then applied (Vuichard et al., 2018). Finally, the particulate and dissolved organic manure-C were
262 assumed to feed the litter and DOC pools, respectively (Fig. S1). Consistent with ORCHIDEE-CNP (Goll et al.,
263 2017), the fractions of particulate and dissolved manure-C were set to 0.9 and 0.1, respectively.

264

265 **2.1.4 Hydrological processes**

266 The representation of hydrological processes is handled in two distinct sub-modules. The first one, the hydrology
267 sub-module, simulates the vertical exchange of water in the atmosphere-vegetation-soil system in each model
268 grid cell, while the second one, the river routing module, simulates the horizontal transfers between grid cells.
269 The hydrology is forced by several meteorological fields such as precipitation and air temperature. In the
270 hydrology module, precipitation is divided into interception and throughfall, the latter being further subdivided
271 into surface runoff and infiltration into the soil. The infiltration rate is controlled by the throughfall rate, the
272 slope of the soil surface and the hydraulic conductivity of the soil which is a limiting factor for infiltration. The
273 distribution of water within the soil is represented by the distribution of soil moisture over the discretized soil
274 profile (de Rosnay et al., 2002, d'Orgeval et al., 2008). The water budget within the soil is thus determined by
275 the infiltration rate and runoff from the top soil, the evaporation and transpiration from the soil, and drainage at
276 the bottom of the soil column. The infiltration rate and percolation through the soil profile are used to compute
277 the advective flux of DOC (equation 2)

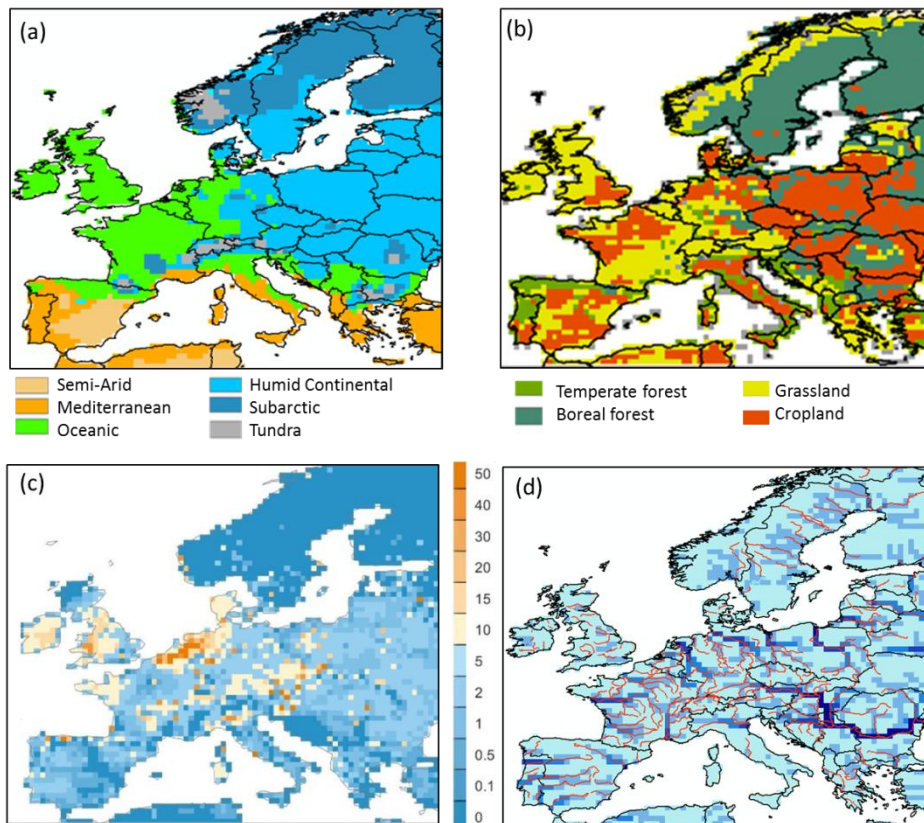
278 The second module deals with river routing and represents the horizontal transfers of water from the soil column
279 to the aquatic system through surface runoff and drainage, and further through the river network and adjacent
280 floodplains (Vorosmarty et al., 2000). Meybeck (1993a,b) found that soils were the major source of DOC to
281 rivers, while autochthonous DOC being negligible at the global scale. Furthermore, autochthonous DOC has a
282 short turnover time and is quickly recycled within the river (Farjalla et al., 2009; Fonte et al., 2013) and,
283 therefore, does not contribute significantly to the net C budget of an entire river system. Since in this study the
284 focus is on the role of fluvial DOC fluxes in the terrestrial C budget, autochthonous DOC is not accounted for.
285 The representation of leaching processes in ORCHILEAK is simplified, the model represents flows of water
286 from land to the stream network only through surface runoff and drainage from bottom soil. Leaching thus
287 occurs either from the topsoil, which in our configuration represents the top 4.5 cm of the soil column, or from

288 the bottom soil, i.e. the lowest 50 cm of the 2 m soil profile. DOC leaching from the top soil is further limited by
289 two reduction factors, a ‘general reduction factor’ and a ‘reduction factor’. The first reduction factor accounts for
290 the fact that some of the runoff represents excess throughfall that never entered the soil and further corrects for
291 the overestimated DOC concentration in the topsoil. The second reduction factor represents the connectivity
292 between streams and their catchment through the extent of the water saturated riparian zone at sub-grid level,
293 which varies with the amount of runoff and water stored in the “slow reservoir” of water, mimicking the
294 groundwater storage. Note that for larger river stretches (stream order 4 and higher), ORCHILEAK simulates the
295 occasional inundation of the river’s floodplains, where DOC production from decomposition of litter and SOC in
296 the top-soil, although being reduced under inundated conditions, feed directly into the DOC pool of the water
297 column. For a detailed description of these features, please refer to Lauerwald et al. (2017).

298 **2.2 Simulations**

299 **2.2.1 Model set-up**

300 **Model domain, land cover and forcing data.** The simulated model domain extends over the area ($4.1 \cdot 10^6 \text{ km}^2$)
301 between 35°N and 70°N latitude and 10°W and 30°E longitude (Fig. 2). This domain includes 5600 model grid
302 cells at $0.5 \times 0.5^\circ$ resolution and encompasses 6 broad climate zones according to the Köppen-Geiger
303 classification from Peel et al., 2017 (Fig. 2a). The dominant PFTs within Europe include croplands (20% mainly
304 C3), grasslands (31%, of which 24% are C3), and forests (39%, of which 16% and 9% are needleleaved
305 evergreen and broadleaved summer-green boreal forests, respectively, while temperate broadleaved summer-
306 green, needleleaved and broadleaved evergreen forests take 8%, 3%, and 3%, respectively) (Fig.2b). The spatial
307 distribution of manure application on grasslands and croplands is shown in Fig.2c. Finally, Fig.2d illustrates the
308 actual river network derived from the HydroSHEDS DEM data (Lehner et al., 2008) and the one corresponding
309 to our river routing scheme at 0.5 degree resolution, highlighting that the representation of the river network is
310 not optimal due to the coarse spatial resolution of our model. This coarse resolution limits the possibility of
311 model validation to the downstream parts of larger river networks. Note further that the mouth of the Rhine is
312 more than 100 km too far east, which further limits model validation for that river.



313
 314 **Figure 2. Spatial distribution for each 0.5° grid cell of the continental European domain of (a) climate zones**
 315 **(according to the Koppen-Geiger classification); (b) dominant plant functional types (PFT) (c) manure**
 316 **application (in $\text{gC m}^{-2} \text{yr}^{-1}$); (d) the routing Network of ORCHILEAK (in blue). The real river network extracted**
 317 **from the European Environment Agency (<https://www.eea.europa.eu/legal/copyright>) is also shown.**
 318

319 The forcing data applied in our study are listed in table 1. They are the same as those used in Lauerwald et al.
 320 (2017) except for the meteorological forcing data and the land cover. The WFDEI meteorological forcing dataset
 321 used in this study was derived by applying the methodology originally used to create the WATCH Forcing Data
 322 (WFD) from the ERA-Interim reanalysis data (Weedon et al., 2014). The dataset has a 0.5° spatial resolution and
 323 a 3-hourly time step from 1978 to 2014. The land cover forcing data set, which gives the areal proportion of the
 324 13 PFTs within each 0.5° grid cell, was taken from Peng et al. (2017). Note that the soil hydrology model in
 325 ORCHIDEE, which we adopted for ORCHILEAK, was developed and calibrated to work with the soil classes
 326 used in Reynolds et al. (1999). We thus kept that data source, while additional soil properties such as pH and
 327 specific soil classes which we defined as “poor soils” (Histosols, Podzols) with lower C turnover times and DOC
 328 filtering were taken from HWSO v1.1. A topographic index, which in ORCHIDEE controls the flow velocity in
 329 the river network of each cell is taken from Vorosmarty et al. (2000). “Floodplains”, defined as the maximum
 330 areal proportion of a grid cell that can be flooded when the river exceeds its bankfull flow, and “Swamps”
 331 representing groundwater fed wetlands in the floodplain, were adopted from the Global Lake and Wetland
 332 database (Lehner and Doll, 2004). Depending on the areal extend of these swamps, a proportion of stream flow

333 is simulated to feed into the soil moisture storage of the grid cell considered. Both parameters have an effect on
 334 the simulated river discharge and soil hydrology in the floodplains. For details, see Lauerwald et al. (2017).

335

336 **Table 1. List of the forcing files used for our simulations, along with their spatiotemporal resolution.**

VARIABLE	SPATIAL RESOLUTION	TEMPORAL RESOLUTION	DATA SOURCE
Rainfall, snowfall, incoming shortwave and longwave radiation, air temperature, relative humidity and air pressure, wind speed.	0.5°	3 hours	WFDEI_GPCC (WATCH Forcing Data (WFD) by making use of the ERA-Interim reanalysis data, Global Precipitation Climatology Centre; Weedon et al. (2014))
Soil texture class	0.5°	-	Reynolds et al., 1999
Soil pH, soil bulk density, poor soil	0.5°	-	HSWD v 1.1 (Fao et al., 2009)
Stream flow directions and topographic index	0.5°	-	STN-30p (Vörösmarty et al., 2000)
Floodplains and swamps	0.5°	-	Guimberteau et al., 2012
River surface area	0.5°	-	Lauerwald et al., 2015
10th, 50th, 90th percentile of the stream reservoir	1°	-	Derived from pre-runs with ORCHIDEE
Land cover	0.5°	-	Peng et al. (2017)

337

338 **Parametrization of hydrological processes.** ORCHILEAK was previously parametrized and validated for the
 339 Amazon (Lauerwald et al., 2017; Hastie et al., 2019; Lauerwald et al., 2020), Congo (Hastie et al., 2021) and
 340 Lena (Bowring et al., 2020) basins. In our study of the European river network, we updated ORCHILEAK with
 341 the more recent hydrology scheme of the recent standard version of ORCHIDEE (svn 5091). This hydrology
 342 scheme has been calibrated against observed runoff at a global scale (Ringeval et al., 2012; Yang et al., 2015).
 343 Furthermore, MacBean et al. (2020) has evaluated the model performance for simulating soil moisture in
 344 temperate ecosystem. This new hydrology scheme features a dynamic surface roughness of the vegetation, which
 345 decreases the aerodynamic resistance near the surface when vegetation cover is low, leading to lower ground
 346 temperatures and thus lower evaporation rates. This adjustment was deemed necessary in order to better capture
 347 the observed mean and seasonal variability of the discharge along the European river network. The two reduction
 348 factors controlling DOC leaching from the top soil to the headwaters streams were also adjusted (see 2.1.4).

349 **Spin-up.** Before the model can be used to simulate C dynamics over the past decades, a spin up is needed to
350 reach an assumed steady state for the C fluxes during the pre-industrial period. This steady state is achieved by
351 spinning up ORCHILEAK for 15000 years. The spin up was realized by recursively looping over 4 years of
352 climate forcing using the WFDEI forcing dataset over the 1979-1982 period (because the first year of the
353 forcing, 1978, is incomplete) and constant land cover and atmospheric CO₂ concentration of 286 ppm
354 (Guimberteau et al., 2018) corresponding to year 1861. After the end of the spin-up, the soil C stock across the
355 entire European continent changed by less than 1% over a century of simulation, which we considered close
356 enough to steady-state.

357 **Transient runs.** Using the steady-state outputs as initial condition, the first part of the transient simulation
358 (1861-1978) was carried out with increasing atmospheric CO₂ concentration, changing land use and land cover
359 and with river routing activated while still looping over 27 years (1979-2006) of the WFEDI forcing dataset.
360 From 1979 onwards, the WFDEI atmospheric forcing data was applied over the entire period covered by this
361 product with the changing land cover map and atmospheric CO₂ values applied for each year of simulation.

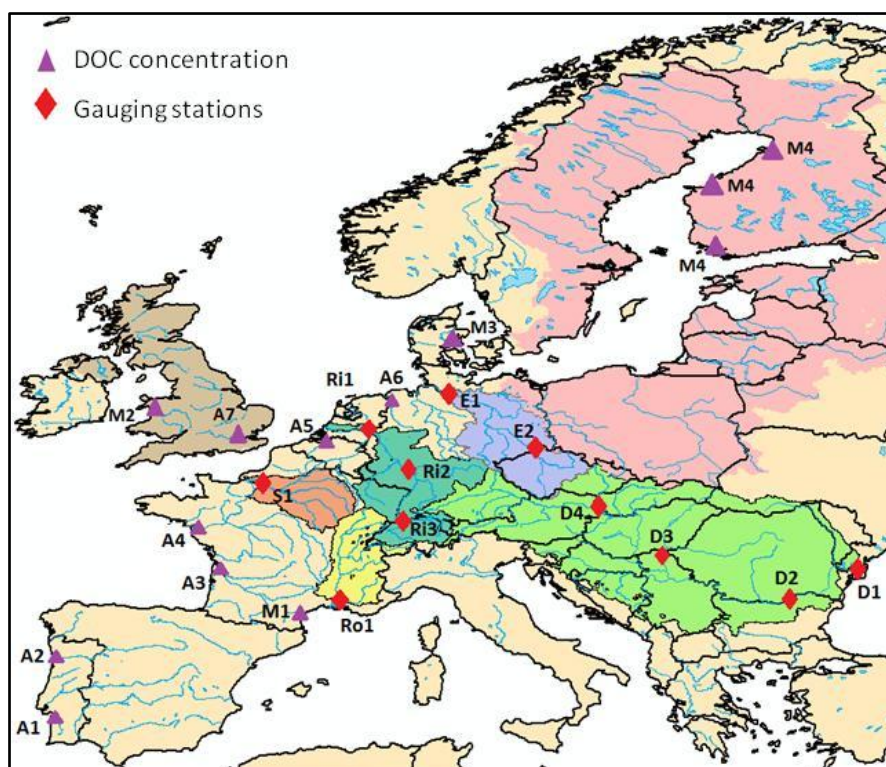
362

363 **2.2.2 Model evaluation**

364 Firstly, the simulated discharges were compared to times series of daily stream flow recorded at eleven gauging
365 stations from “The Global Runoff Data Center (GRDC), 56068 Koblenz, Germany” dataset. For comparison,
366 both observed and simulated discharges were aggregated at the monthly temporal resolution over the years 1980
367 to 2006. Note that the river network in ORCHILEAK does not always match the real river network. The selected
368 gauging stations were assigned to the cell best representing the parts of the river network to which the sampling
369 location corresponds. However, important correction had to be performed for the most upstream stations in the
370 Rhine and the Elbe river network. The period 1980 to 2006 was chosen based on the GRDC data coverage.

371 Model performance was further evaluated with respect to several variables of the terrestrial C cycle. Firstly,
372 simulated Net Primary Production (NPP) was compared to two different data products. The first one, the
373 CARbon DAta MOdel fraMework (CARDAMOM; Bloom et al., 2015) built from model data fusion analysis at
374 1° resolution. The second one is the Global Inventory Modeling and Mapping Studies (GIMMS) at 0.5°
375 resolution based on AVHRR and MODIS sensors. GIMMS uses several atmospheric forcing data set to derive
376 NPP. Those are CRUNCEP version 4 P1 and P2 (Rainfall, cloudiness, relative humidity and temperature taken
377 from the CRU (Climate Research Unit), while the other fields such as air pressure, longwave radiation, wind
378 speed are directly derived from NCEP (National Center for Atmospheric Research)), ECMWF (European Centre
379 for Medium-Range Weather Forecasts), MERRA2 (the Modern-Era Retrospective analysis for Research and
380 Applications, Version 2) and NCEPR2 (<https://www.esrl.noaa.gov/psd/>). For our comparison, we calculated the
381 average of the NPP obtained with these five atmospheric forcing files. The NPP values from ORCHILEAK and
382 GIMMS were averaged over the period 1982-2006 while CARDAMOM only covers a shorter time period
383 comprised between 2001 and 2010. Modelled NPP was then compared to the NPP data products at the European
384 scale and at the scale of five large European basins for which we also evaluated the simulated river discharge and
385 DOC fluxes, and which taken together, represent 19 % of the model domain (Fig.3): the Danube, Rhine, Elbe,

386 Rhone and Seine. All five basins are located in an oceanic or humid continental climate (Fig.2a) although the
 387 Rhone basin extends further into the Mediterranean climate zone. The basin characteristics according to land
 388 cover types are as follows: the Danube and the Elbe basins have both a high proportion of croplands (around
 389 40%), the remainder being mostly covered by grasslands and boreal forests. The Rhone is covered by 50% of
 390 grasslands, while in the Seine basin croplands reach 50%. The Rhine has a more diverse land cover with a
 391 substantial proportion (about 30%) of boreal (10 %) and temperate (20 %) forests, 35% of grasslands and 25% of
 392 croplands. See table S2 for further details.



393
 394 **Figure 3. Map of continental Europe delineating the (group of) catchments of focus in this study and the location of**
 395 **observed discharge and DOC concentrations. Catchments, from west to east are: All UK (light brown), Seine**
 396 **(orange), Rhone (yellow), Rhine (dark green), Elbe (violet), All Baltic (pink) and Danube (light green). Observations**
 397 **include GRDC stations (red diamonds) in the Seine (S1-Poses), Rhone (Ro1-Beaucaire), Rhine (Ri1-Lobith, Ri2-Main**
 398 **in Frankfurt, Ri3-Basel), and Danube (D1-Ceatal Izmael, D2-Svistov, D3-Tisza in Senta, D4-Bratislava) catchments,**
 399 **as well as river stations where DOC concentrations were measured (purple triangles): A1-Douro, A2-Sado, A3-**
 400 **Gironde, A4-Loire, A5-Scheldt, A6-Ems, A7- Wales, A8-Thames, M1-Tech, M2-Wales, M3-Denmark, M4-Finland**
 401 **(Abril et al 2002, Mattsson et al., 2008).**

402
 403 The soil temperature is compared to the soil temperature generated using data from the European Centre for
 404 Medium-Range Weather Forecasts reanalysis ERA5 dataset (Munoz-Sabater et al., 2021). The soil heterotrophic
 405 respiration (SHR) is compared against the data-driven global SHR dataset published by Yao et al. (2020). The
 406 global SHR data set was produced using a Random Forest algorithm, up-scaling from 455 data points from the
 407 Global Soil Respiration Database (SRDB 4.0) based on gridded fields of climatic, edaphic and productivity
 408 related variables as predictors (Yao et al., 2020). We compared the results of ORCHILEAK with the average,

409 minimum and maximum values of SHR estimated by Yao et al. (2020). SOC from the Harmonized World Soil
410 Database (HWSD) was used to evaluate the simulated SOC stocks. HWSD is a global soil database that
411 contains up-to-date information on a large range of soil properties. For instance, this dataset reports the organic
412 carbon content in the soil as well as the soil bulk density. The bulk density in HWSD was calculated in two
413 different ways. The first one follows the method described in Saxton (1986) where the bulk density is related to
414 the soil texture - an approach tending to overestimate density in high porosity soils or in OC rich soils. The
415 second method uses the SOTWIS database in which the bulk density is calculated as a function of soil type and
416 depth. In this database, all variables are reported for the topsoil (0-30cm) and the sub-soil (30-100cm) horizons.
417 For comparison purposes, our simulated SOC stocks were thus integrated over the same depth intervals. We
418 further assessed the extent to which our model can reproduce the main features in observed soil DOC profiles.
419 To that end, we compared our simulated DOC profile averaged over the entire European forest biome against the
420 one established by Camino et al. (2014) on the basis of a synthesis of local measurements. Although there are
421 many studies on DOC concentrations in the soil, we selected the one by Camino et al. (2014) because it provides
422 a synthesis at the pan-European scale, and is thus ideal to extract “representative” concentration profiles over a
423 sufficiently large domain, compatible to the regional scope of our study. Unfortunately, similar synthetic profiles
424 based on observations have not been constructed for croplands and grasslands.

425 The key variables of interest in our study are the DOC leaching flux from the soil and the DOC export flux to the
426 coast. These fluxes require accurate simulation of the water discharge fed by runoff and drainage as well as of
427 DOC concentrations in the leaching flux and in the riverine flux. For the leaching flux, our simulation results
428 were compared to measured fluxes reported by Kindler et al. (2011) across different locations in Europe.
429 Because the observed DOC leaching fluxes from both top and bottom soil reported by Kindler et al. (2011) are
430 based on local measurements that are not easily comparable to simulated fluxes at the coarse spatial resolution of
431 our model (0.5° or about $2 \cdot 10^3 \text{ km}^2$ at the corresponding latitude), we consider the comparison against measured
432 river DOC fluxes more relevant for our purpose, as rivers are good integrators of mean, larger-scale catchment
433 properties. For the riverine export fluxes, we assessed the modeled discharges and DOC concentrations
434 separately. For evaluation of stream DOC concentrations, DOC data were extracted from the GLObal RIVER
435 CHEMISTRY database (GLORICH, Hartmann et al., 2014) for the Rhine and Elbe basins and from the “Eau de
436 France” database for the Seine and Rhone basins. These data were complemented by river DOC concentrations
437 reported by Abril et al. (2002) for 9 river mouths (Sado, Thames, Ems, Scheldt, Gironde, Douro, Loire, Elbe and
438 Rhine), and by Mattsson et al. (2008) for several river basins located in Finland, Denmark, Wales and France.

439 **3 Results and discussion**

440 **3.1 Model evaluation at pan-European and catchment scales**

441 **3.1.1 Discharge**

442 Figure 4 compares the simulated discharge against observations for selected stream gauging stations (section 2).
443 Those stations are located near the mouth of large rivers (Danube, Rhine, Rhone, Elbe and Seine) but also
444 include a few locations further upstream the same rivers or at major tributaries (Fig.3). The comparison is

445 performed for the period 1990-2000, except for the Rhone at Beaucaire and the Danube at Svistov for which the
446 observed stream gauge data cover only a shorter period. Overall, the model reproduces the observations well,
447 both in terms of amplitude and seasonality, except for the Elbe at Neu Darchau, for which the temporal
448 variability is well captured but the absolute discharge is overestimated.

449 Note that the simulated catchment area often diverges (by -25% to +30 %) from the observed value due to the
450 coarse resolution ($0.5^{\circ} \times 0.5^{\circ}$) of ORCHILEAK (Table S3). As a result of the model resolution, smaller tributaries
451 are not represented individually and each grid cell was fully assigned to one larger river basin. The effect of the
452 resolution is also shown in Fig.2d which compares the observed and modeled river network. Discrepancies
453 between model and real world catchment area will translate into proportional biases in discharge simulation.

454 Furthermore the 0.5° resolution is too coarse to be able to represent perfectly the pathways of the river. Our
455 model tends more often to underestimate the catchment area, while its yearly mean discharge is overestimated,
456 except at the Beaucaire station along the Rhone River. The bias can be significant and cannot be explained by
457 the model resolution alone.

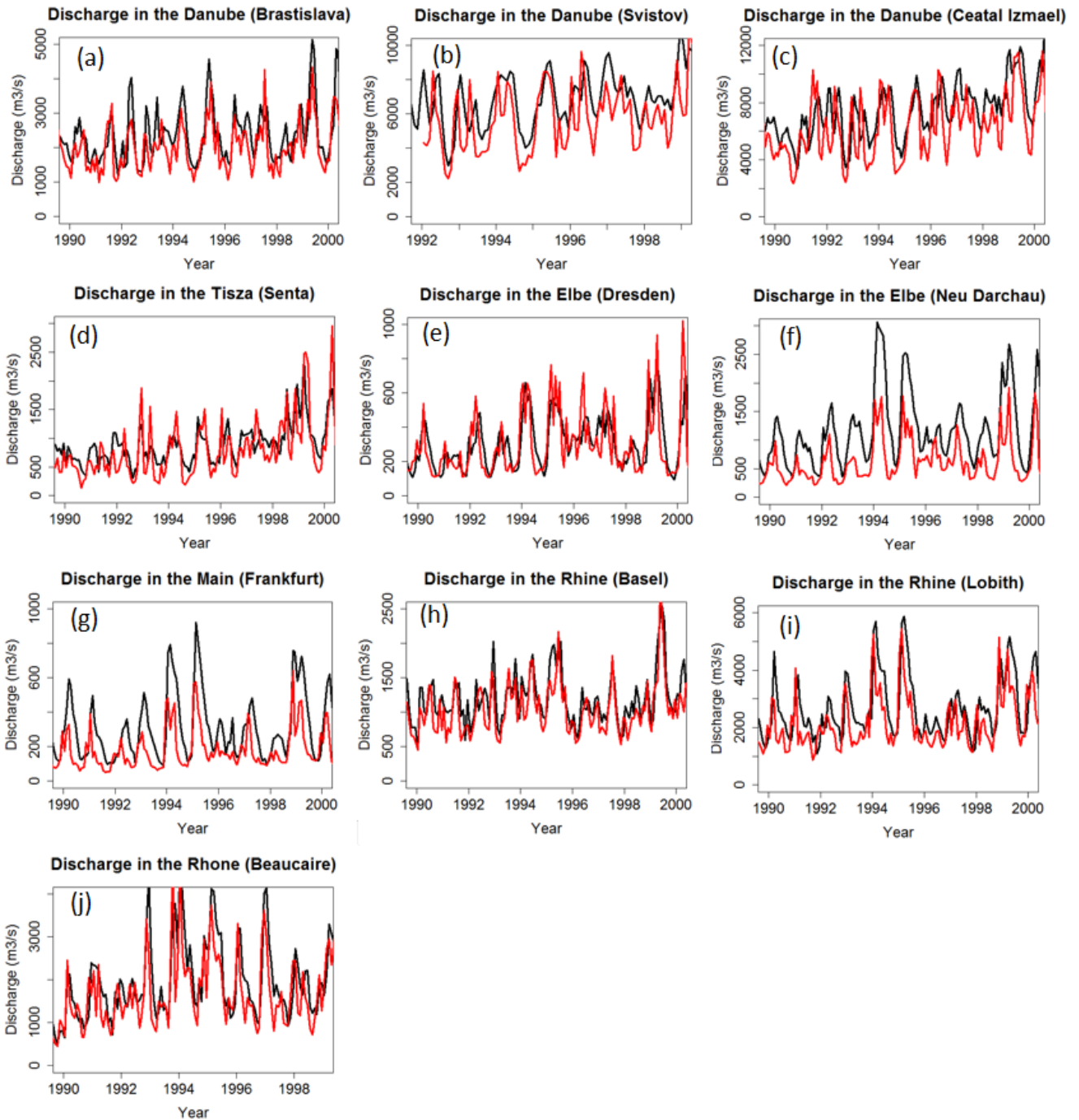


Figure 4. Modeled (black) and observed (red) time series of discharge at the GRDC gauging stations in the Danube (a-c) and its tributaries (d), Elbe (e-f), Rhine and its tributaries (g-i) and Rhone (j). Note the different time periods of measurements. See Figure 3 for exact location.

To evaluate model performance for discharge, we used the Pearson's coefficient of determination (R^2) and the Nash Sutcliffe modeling efficiency (NSE, Nash and Sutcliffe (1970)). The R^2 only accounts for the correlation with regard to the temporal variability. With R^2 values comprised between 0.43 and 0.62 for all stations, we conclude that the observed seasonality of the discharge along large European rivers is reasonably well reproduced by the model. The NSE not only accounts for the correlation between observed and simulated temporal signals, but also for the model's ability to reproduce absolute discharges. The statistics confirm our previous observation that the model generally overestimates discharges (low NSEs) except for stations Elbe in Dresden, Rhone in Beaucaire, Rhine in Basel and Danube in Bratislava where both the mean and temporality are well captured. Two stations have negative NSE values, which means that the error variance estimated by the model is significantly larger than the variance of the observations; in others words, the difference between model and

observations is significant. The mean error (%), that is, the weighted difference between the average from the model and the one from observation, confirms that low NSEs are mostly due to overestimated discharges, which is further demonstrated by high mean errors. More results for other European catchments can be found in table S3.

475

3.1.2 NPP, SHR, soil temperature, biomass and soil organic C stocks

We briefly compare simulated NPP with the gridded observation-based products GIMMS and CARDAMON (section 2.2.2) as C fixation by the vegetation exerts an important control on DOC stocks in the soil and thus on DOC leaching. We first perform our comparison over a large domain comprised between -10° and 30° in longitude east and 35° and 70° in latitude north - covering the area from Ireland to the Western Black Sea (where the Danube flows into) and from the south of Spain to the north of Scandinavia. Over this area (referred to as “Europe” from here onwards), the modeled yearly averaged NPP amounts to $445 \text{ gC m}^{-2} \text{ yr}^{-1}$, a value in remarkable agreement with both GIMMS and CARDAMOM estimates of $430 \text{ gC m}^{-2} \text{ yr}^{-1}$ and $460 \text{ gC m}^{-2} \text{ yr}^{-1}$, respectively. Those two datasets are entailed with an uncertainty that we assume similar to that reported for the MODIS dataset, i.e. 20% (Turner et al 2006). The total living biomass in Europe is simulated at 15.5 PgC or 2.3 kgC m^{-2} . This value is in good agreement with the recent estimate by Avitabile and Camia 2018, which report a biomass stock at around 16 PgC. We estimate that the total soil carbon stock amounts to 58 PgC. Averaged over the first meter of the soil horizon, this corresponds to a value of 9.5 kgC m^{-2} which is comparable to that of HWSD (6 kgC m^{-2}) when using the SOTWIS method to compute the bulk density, but significantly lower when applying Saxton's method (22 kgC m^{-2}), plausibly because the latter overestimates the bulk density in OC-rich soils (Kochy et al., 2015). Results at the catchment scale are described in the supplementary section.

Figure 5a shows the comparison of simulated vs. data driven estimates of soil temperature. Soil temperature is overall well represented with a simulated mean temperature of 8.4° C against 9.3° C after ERA5. The overall slight underestimation is due to a substantial underestimation of soil temperatures in the northern regions. Furthermore, this underestimation is more important in the winter (January, February and March) with a difference relative to ERA5 values reaching 3.5° C , while in summer (July, August and September) this difference amounts to only 0.5° C . This underestimation is due to the poor representation of the isolating effect of the snow cover in ORCHIDEE (Wang et al., 2013).

The comparison of simulated SHR against Yao et al.'s estimate is shown in Figure 5b. Over Europe, ORCHILEAK underestimates the SHR compared to Yao et al.'s estimates by about 14%, with a simulated average of $312 \text{ gC m}^{-2} \text{ yr}^{-1}$ against an average of $363 \text{ gC m}^{-2} \text{ yr}^{-1}$ (range from 317 to $417 \text{ gC m}^{-2} \text{ yr}^{-1}$) estimated by Yao et al. (2020) for the period 1985-2013. Looking at specific climatic regions, some regions are well represented in ORCHILEAK, as the Mediterranean and humid continental regions with a mean SHR of 371 and $363 \text{ gC m}^{-2} \text{ yr}^{-1}$, against 385 and $354 \text{ gC m}^{-2} \text{ yr}^{-1}$ from Yao et al., respectively. SHR in semi-arid and tundra regions are on the contrary around 50% lower than Yao et al.'s estimate. For the tundra region the underestimation in SHR is consistent with an underestimation of the NPP (see table S4).

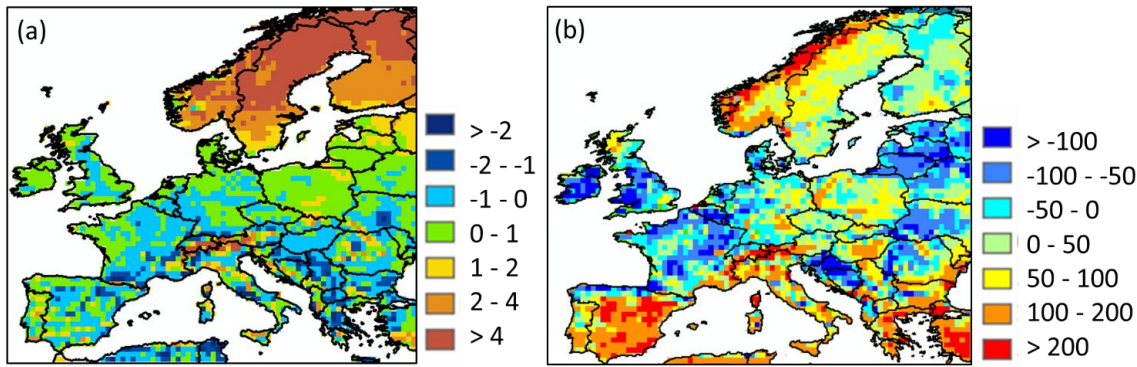


Figure 5. Difference in (a) simulated soil temperature (in °C) against values reported by ERA5; (b) simulated soil heterotrophic respiration (in $\text{gC m}^{-2} \text{yr}^{-1}$) against values reported by Yao et al. (2020).

510 3.1.3 Soil DOC stocks

Comparison between observed and modeled DOC stocks and fluxes is more difficult than for biomass and SOC because those have not been assessed at large spatial scales. Nevertheless, representative soil DOC concentration profiles for coniferous and broadleaved forests of Europe have been compiled by Camino et al. (2014). These profiles were used to evaluate our model. Overall, we found that ORCHILEAK slightly overestimates DOC concentrations, especially in the very topsoil layers with modeled values of around 100 mg l^{-1} against $40\text{-}60 \text{ mg l}^{-1}$ in the observations (Fig. 6). We also simulated higher concentrations in broadleaved forests than in coniferous forests while Camino et al. (2014) obtained the opposite. When integrated over the first meter of the soil horizon of forested ecosystems (28 % of the European land area), the modeled and observed DOC stocks amount to 22.2 and 11.3 gC m^{-2} , respectively. Above, we have shown that over Europe SOC stocks were underestimated while the average DOC concentrations in the soil over all European forests are here overestimated. One explanation for the underestimation of SOC stocks and the likely overestimation of DOC stocks is thus that SOC decomposition rates in the new soil carbon module may be slightly too high. It is however difficult to generalize this conclusion because of the lack of synthesis data for other land cover types, especially croplands and grasslands which together represent about 50 % of the total European land area. Modeled DOC stocks averaged over broad climate regions reveal highest values for the oceanic climate with 32 gC m^{-2} and the Mediterranean climate with 26 gC m^{-2} . Semi-arid and humid continental climates have similar stock densities of respectively 17.5 and 20 gC m^{-2} and it is in the coldest climates (subarctic and tundra) that we find the lowest DOC stock densities of around 8 gC m^{-2} .

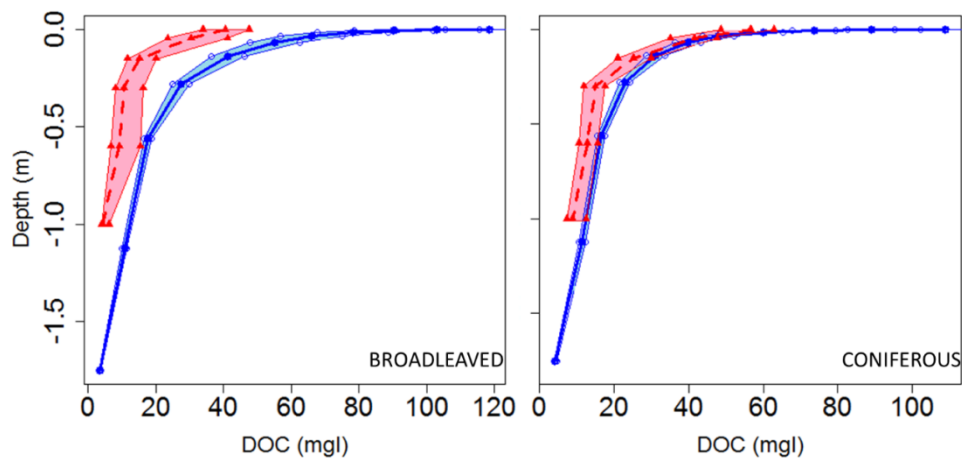


Figure 6. Modelled (blue) versus observed (red dashed) DOC concentration profiles averaged over the soils of the European Coniferous and Broadleaved forest biome. Data from Camino et al. (2014). The shaded area represents the 95% bootstrap confidence interval for model and observations.

3.1.4 DOC leaching fluxes

The model simulates a yearly-mean DOC leaching flux over Europe of $14.3 (\pm 10) \text{ TgC yr}^{-1}$ (Fig 7), the standard deviation being here coarsely approximated by spatial variability. The average area specific flux rates amounts to $2.6 (\pm 2.5) \text{ gC m}^{-2} \text{ yr}^{-1}$. We compared DOC leaching fluxes with site level observations from Kindler et al. (2011), across 17 local measurements, each sampled fortnightly during the period October 2006 until March 2008. Comparing model results at 0.5° resolution to point measurement is complicated, and thus in this section, we compare only our model-averaged result against the 17-site average from Kindler et al. (2011). Our modeled average of $2.6 (\pm 2.5) \text{ gC m}^{-2} \text{ yr}^{-1}$ is of the same order of magnitude as the observed one ($4.2 \text{ gC m}^{-2} \text{ yr}^{-1}$). Although the modeled mean is about 38 % lower than the one measured, the standard deviation representing the spatial variability in simulated DOC leaching fluxes over all our model grid cells encapsulate the observational mean, highlighting a significant heterogeneity that is difficult to embrace with local measurements alone. This comparison must be taken cautiously because of the limited number of observations and the resolution of our model. Furthermore, DOC leaching flux at the coast is generally not well represented. The reason is that DOC leaching fluxes are normalized by the area of the whole cell. The area normalized flux at the coast is thus often lower.

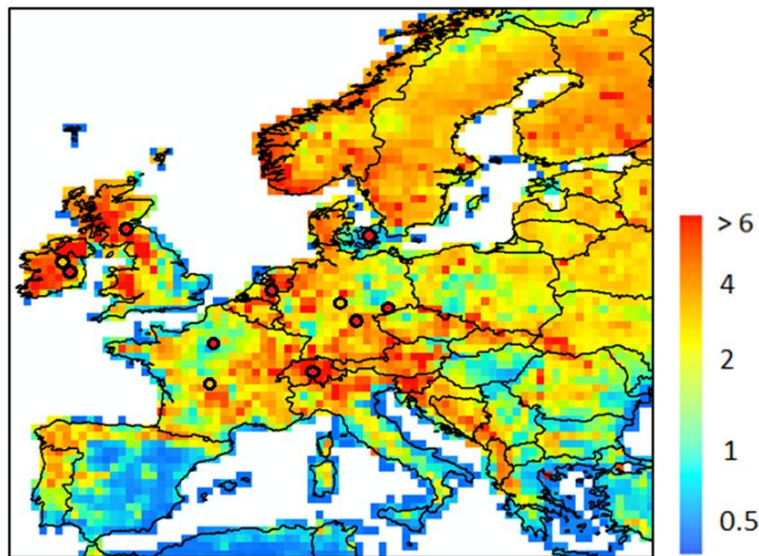
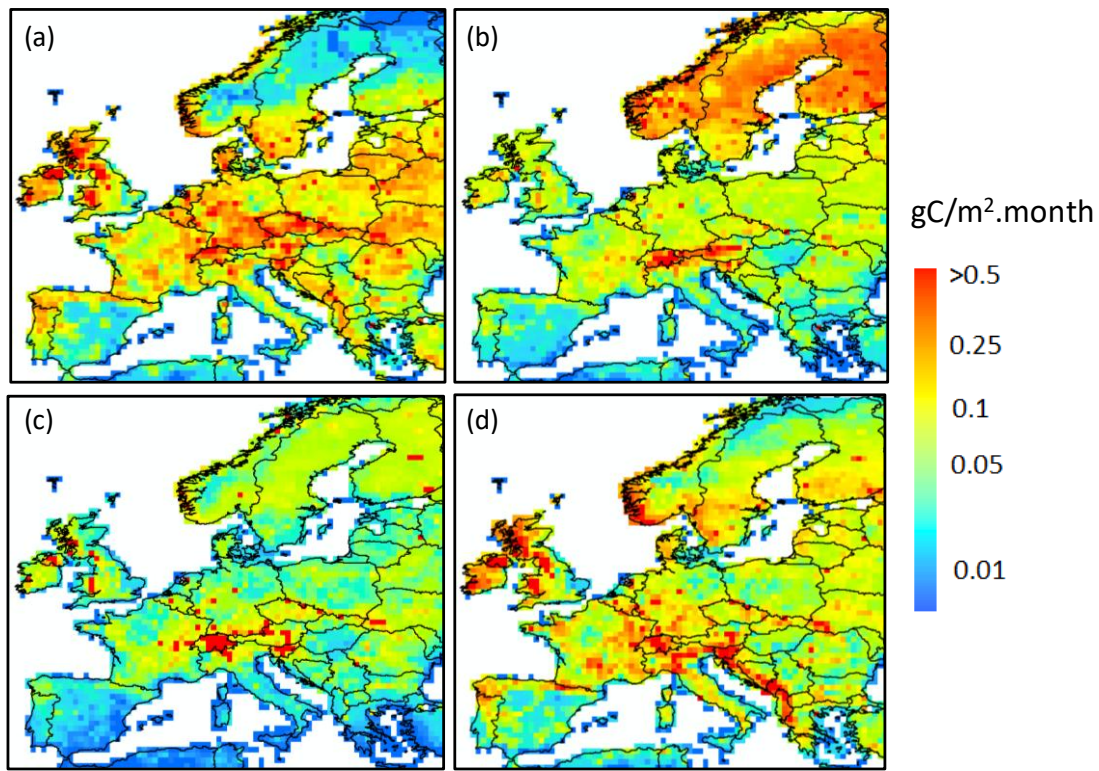


Figure 7. Modelled yearly mean terrestrial DOC leaching flux (period 1979-2006) to the river European river network (in $\text{gC m}^{-2} \text{ yr}^{-1}$). The local observations from Kindler et al., 2010 are also reported, using the same scale. Note that the local observations cover a much shorter time period and may not be representative of the whole year.

The seasonal distribution of the DOC leaching flux is shown in Fig. 8. On average, the leaching flux per season averaged over Europe amounts to 1.6, 1.3, 0.5 and $1.4 \text{ TgC month}^{-1}$ in winter, spring, summer and autumn, respectively. If we exclude the high latitude and high altitude regions (Scandinavia, the Alps), a clear seasonality is observed with the lowest fluxes in summer and spring and the highest fluxes in winter and autumn. In the high latitude/altitude regions, the pattern is different with highest fluxes in spring which extends to the summer in the Alps, and corresponds to the snowmelt period. The highest fluxes per unit area are simulated in Scandinavia during the spring season, even though peatlands are not represented in the model. Some regions are leaching hotspots such as the Alps throughout the year, the West Balkans during autumn and the Western flank of the UK in autumn and winter.



560 **Figure 8.** Seasonal distribution of the terrestrial DOC leaching flux ($\text{gC m}^{-2} \text{ month}^{-1}$) for (a) Winter, (b) Spring, (c) Summer and (d) Autumn, averaged over the period 1979-2006. A logarithmic scale is used to better highlight the spatiotemporal gradients.

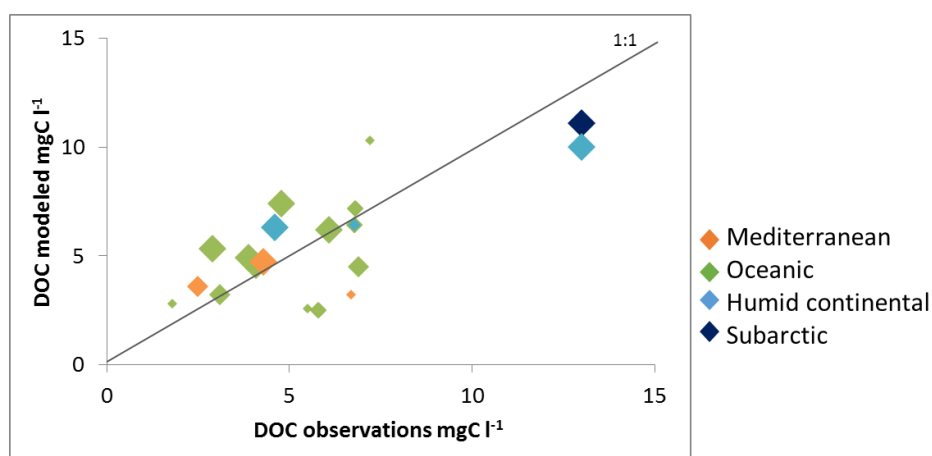
3.1.5 Fluvial DOC decomposition and export fluxes

The export of DOC from the European river network to the coast is arguably the best monitored variable against which our model can be evaluated. Using this flux to build confidence in our estimate of the terrestrial DOC leaching requires an assessment of the DOC degradation within rivers, a process that is controlled by the hydrology and the half-lives of reactive DOC compounds. In the model, the first-order decomposition rates at a given temperature of 28°C are equal to 0.3 d^{-1} and 0.01 d^{-1} for the labile and refractory DOC pools, respectively. Based on those values and the simulated distribution of labile and refractory DOC, the estimated bulk decomposition rate constant averaged over the entire model domain is equal to 0.05 d^{-1} , which corresponds to a half-life for riverine DOC of about 14 days (Table 3). This rate constant varies across Europe but always remains within the same order of magnitude, with half-lives ranging from 6 to 20 days ($0.035\text{-}0.122 \text{ d}^{-1}$). These decomposition rates are in good agreement with the average rate reported by Berggren and Al-Kharusi (2020) of 0.037 d^{-1} based on field experiments carried out at multiple river sampling locations across Europe. We thus conclude that DOC decomposition rates used in ORCHILEAK are reasonable, and fluvial DOC fluxes are a valid proxy to evaluate simulated DOC leaching fluxes.

575

Table 3. Estimated river DOC decay rates applied in ORCHILEAK. Values are reported for four large river catchments and for the six dominant climate zones

	REGIONS	DECAY RATES (day ⁻¹)
BASIN	Rhine	0.074
	Danube	0.043
	Meuse	0.056
	Rhône	0.072
CLIMATE ZONE	Semi-arid	0.035
	Mediterranean	0.046
	Oceanic	0.053
	Humid continental	0.048
	Subarctic	0.064
	Tundra	0.122



580 **Figure 9. Modelled river DOC concentration against observed values. The color code indicates the dominant climate zone for each catchment while the size of the diamond is proportional to the catchment area according to the following classes: < 10 000 km², < 50 000 km², < 100 000km² and > 100 000 km². See table S4 for further details.**

Figure 9 compares modeled versus observed multi-annual mean riverine DOC concentration at specific locations or within a group of small river catchments. Local DOC measurements include data near the mouth of the Rhine, Elbe, Rhône and Seine rivers (discharge, DOC concentration and fluxes for the Rhine and Seine in figure 10). In addition, Abril et al. (2002) report DOC concentrations measured at nine river mouths discharging along the Atlantic façade and the North Sea, three of which (Rhine (NL), Scheldt (BE) and Gironde (F)) resolve the seasonality while the other six (Elbe (GE), Ems (GE), Thames (UK), Loire (FR), Sado (P), Douro (P)) only rely on a single measurement per year. Both GLORICH and Abril et al. (2002) report DOC concentrations at the mouth of the Rhine and the Elbe but their values diverge because in addition to analytical uncertainties, the sampling period and data density are not the same. Measured values are equal to 4.3 and 2.9 mg C l⁻¹ for the Rhine and 4.6 and 6.1 mg C l⁻¹ for the Elbe, respectively highlighting inherent variability in observational data. To complement these local samplings, we also compared our simulated DOC concentrations with those of Mattson et al. (2008) for several groups of catchments in Finland (9 spread over the whole country), Denmark (10 draining into Horsens fjord), the UK (10 draining into the River Conwy) and France (5 draining into the River Tech). All measured DOC concentrations

ranged from 2.5 mg C l⁻¹ to 10 mg C l⁻¹ except in two regions in the north (Finland and basins flowing into the Baltic sea) where concentrations exceeded 10 mg C l⁻¹. For most of the data, the model slightly overestimated the river DOC concentrations. The model results also suggest that DOC concentrations broadly increase with latitude, with the higher values found in humid continental and subarctic climate and the lower ones in the Mediterranean climate, a result in agreement with the observations from Mattson et al. (2008). Such pattern possibly results from decreasing mean annual air temperature and runoff in Northern Europe that favor incomplete decomposition of litter and soil DOC, thus favouring DOC production in the soil, while at the same time DOC turnover rates in the soils are decreased. Also the increased abundance of forests, and in particular coniferous forests, is a valid explanation for higher DOC leaching (Lauerwald et al. 2012). However, it is important to keep in mind that we are not representing peatlands, suggesting that we could lack part of the DOC leaching in subarctic and tundra regions leading to even higher DOC fluxes further in the North. Finally, the comparison reveals that model performance tends to improve with catchment size, likely reflecting the difficulty to capture the DOC dynamics at the small scale with the current resolution of ORCHILEAK. But overall, our model is capable of reproducing observed yearly mean DOC concentrations for a wide range of river basins spread between Finland and Portugal.

610

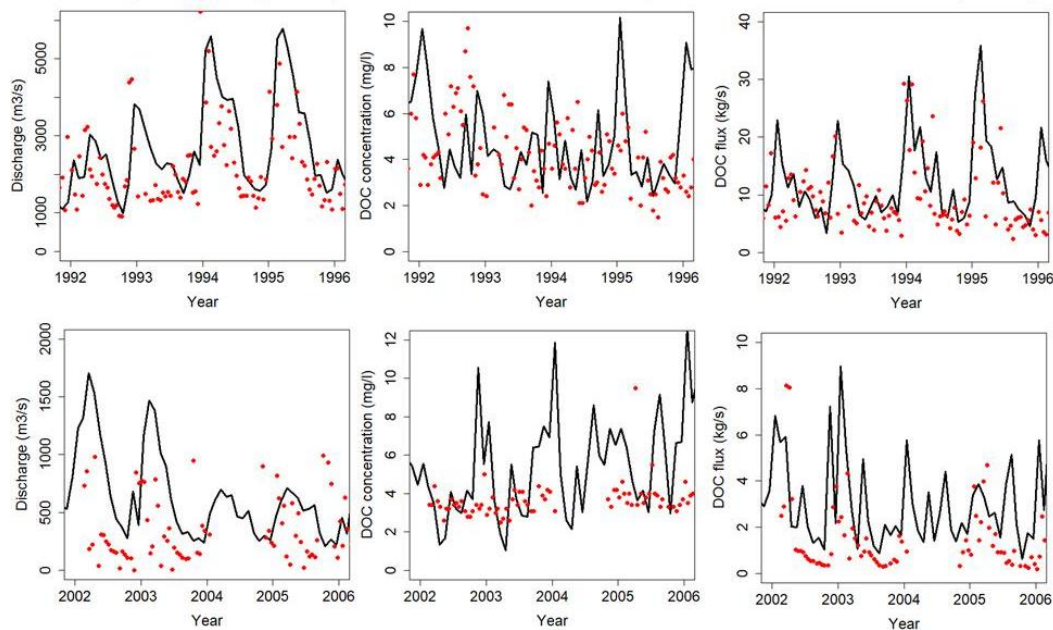


Figure 10. Time series of discharge (left), DOC concentration (middle) and DOC fluxes (right) in the river Rhine at Lobith (top row, period 1992-96) and in the Seine at Poses (bottom row, period 2002-2006. See figure 3 for location of stations. (Black lines for ORCHILEAK and red dots for observations)

615

The temporal evolution of observed river DOC fluxes is only available at four stations (Rhine, Elbe, Rhône and Seine) where DOC time series have been recorded over multi-annual periods (Rhine and Seine illustrated in Fig. 10). In term of inter-annual variability (IAV), riverine DOC fluxes present the highest variability with a coefficient of variance (COV) of 0.62 for the Seine and 0.57 for the Rhine. For comparison, IAV of discharge and riverine DOC concentration shows COVs of 0.60 and 0.51 for the Seine and 0.40 and 0.45 for the Rhine, respectively. The higher IAV for the flux is due to a tendency of higher concentrations coinciding with higher discharge, which is due to the flushing effect where higher discharges follow higher amounts of runoff from top-soils rich in DOC. The multi-year mean modelled DOC fluxes are estimated for the Rhine, Elbe, Rhone and Seine at 11.9, 7.2, 8.8 and 3.2 kg s⁻¹, respectively. The observations amount respectively to 7.9, 3.6, 4.6, 1.6 kg s⁻¹. For all stations, the model thus slightly overestimates fluvial DOC fluxes, which is not surprising since the model tends to overestimate the discharge. At these four stations, ORCHILEAK also slightly overestimates river DOC

625

concentrations except for the Seine where concentrations are largely underestimated and discharge largely overestimated. In terms of temporal correlation, the simulated DOC flux for the Rhone compared to the observed one yields a R^2 of 0.6 and a mean error of 92% (results for the Seine, Elbe and Rhine are reported in supplementary table S6). In figure 9, we clearly see a large overestimation of the temporal variability in DOC concentrations and this could lead to an overestimation in DOC fluxes since there is a positive relationship between concentrations and discharge. The overestimation of DOC concentrations and consequently of DOC fluxes could be due to high DOC leaching.

The overestimation of DOC fluxes can also be due to the fact we choose to not recalibrate the hydrology scheme but instead we optimized the model for the discharge by adjusting the surface roughness of the vegetation (section 2.2.1). Since those four stations are all located in the same region with the same type of land cover (Western Europe), two other locations have been selected: England and the Baltic Sea. For those two locations, there are no time series data for DOC flux but some studies have measured DOC concentrations/fluxes. Worrall et al. (2012) estimated DOC concentration across UK and Fransner et al. (2016) reported modelled DOC concentrations for all the catchments flowing into the Baltic Sea.

Finally, although the model-data comparison points to a slight overestimation of the river DOC export flux, our pan-European estimate amounts to 12.3 TgC yr^{-1} . This estimate is in fact about 35 % lower than the one reported in another model study by Li et al. (2019), based on TRIPLEX-HYDRA, a process-based model for which the DOC export flux reaches 19.3 TgC yr^{-1} . Li et al. (2019) applied the model at the global scale and simulation results were primarily evaluated against observations in the world-largest rivers and for Europe only included the Volga River. Li et al. (2019) then applied the model for multiple rivers in Europe such as the Danube, the Po, and the Elbe. Despite these different scales of analysis, the export fluxes predicted by both models fall within the same order of magnitude.

645

3.1.6 Manure implementation

The implementation of manure significantly affects DOC leaching from grasslands and croplands (Fig. 11) which cover more than half of the studied region. The average annual input rate of manure into the soil is around $2.5 \text{ gC m}^{-2} \text{ yr}^{-1}$ (Fig. 2c). With manure implementation, the DOC leaching rate increase drastically (average of +72% compared to the DOC leaching without manure), in particular in the oceanic and humid continental climate regions, where the average DOC leaching rate changes from 1.6 to $2.7 \text{ gC m}^{-2} \text{ yr}^{-1}$ and 1.7 to $2.5 \text{ gC m}^{-2} \text{ yr}^{-1}$, respectively. For the whole of Europe, manure implementation leads to an increase of total DOC leaching into the river network from 9.8 to 14.3 TgC yr^{-1} (fig 11 (a-b)). Figure 11 (d) shows that the application of manure increases DOC leaching in particular in winter (January, February and March) while in summer (July, August and September) the increase is relatively low. In ORCHILEAK, the manure derived DOC first enters the topsoil. There, a part of it is decomposed, and the rest is transported to deeper soil layers with percolating water. Finally, a variable part of the DOC derived from manure is flushed out of the soil column with the surface runoff and belowground drainage. As manure enters first the topsoil, one could expect that it would increase mainly the DOC leaching from the topsoil. However, our results show that the application of manure does not influence the ratio of DOC leaching through surface runoff vs. belowground drainage. Over Europe, the average increase in top-soil DOC leaching due to manure is equal to half of the total increase, the rest of the increase being contributed by the drainage.

660

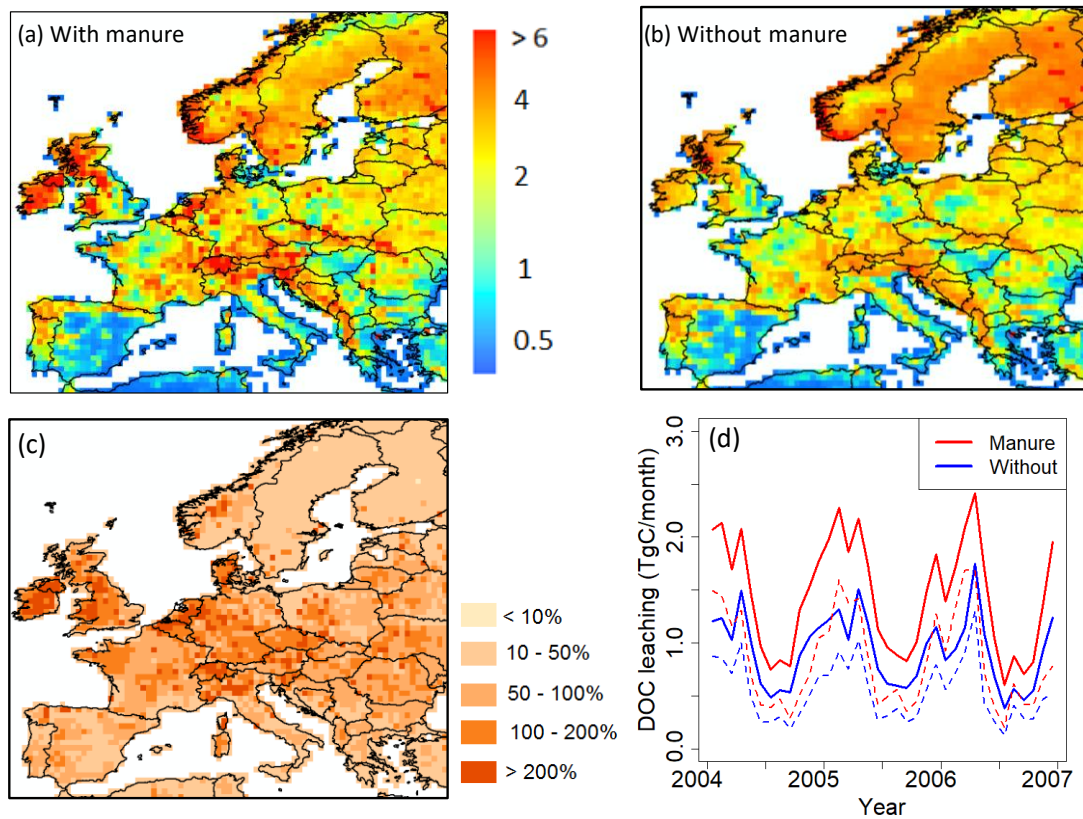


Figure 11. Comparison of modeled yearly mean terrestrial DOC leaching flux (period 1979-2006) to the river European river network (in $\text{gC m}^{-2} \text{yr}^{-1}$), with (a) and without (b) the representation of manure application. (c) Increase of DOC leaching in percentage compared to DOC leaching without the manure implementation. (d) Comparison of total DOC leaching (solid line) and DOC leaching through runoff only (dashed line) over all of Europe with and without manure application (years 2004-2006).

665

3.2 European-scale DOC leaching dynamics

3.2.1 Drivers of DOC leaching

Here, we analyze what controls the spatial distribution and temporal variability in DOC leaching. While the grid cell and the basin scales were the most relevant for the model evaluation, when searching for potential drivers of soil DOC leaching, such as temperature, runoff and drainage (driven by precipitation), a climatologic segmentation of the European domain can help to better explain the impact of these drivers. Figure 12 shows seasonal variability of DOC leaching and total runoff (surface runoff plus drainage) in different climate zones of Europe, revealing a clear and consistent relationship between those two fluxes. The seasonal peak in DOC leaching consistently occurs in winter while minimum values are found during summer. These results suggest that both spatial and temporal variability in leaching are correlated to total runoff.

675

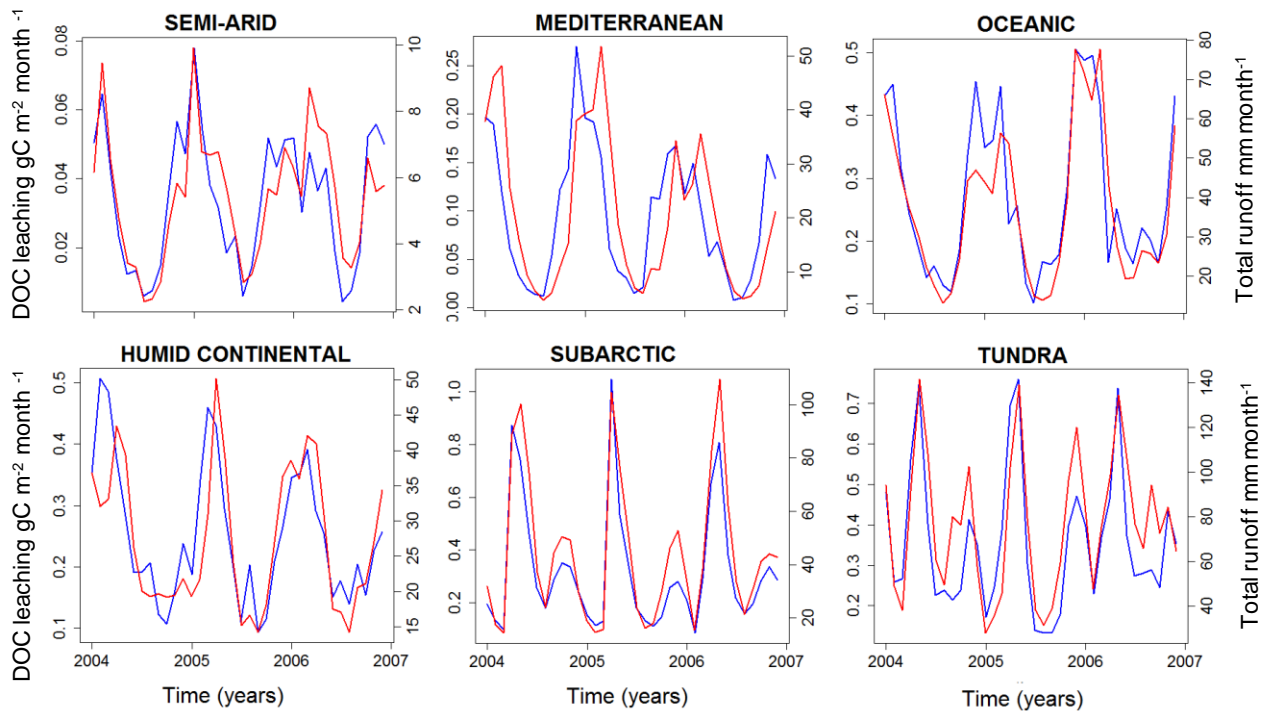


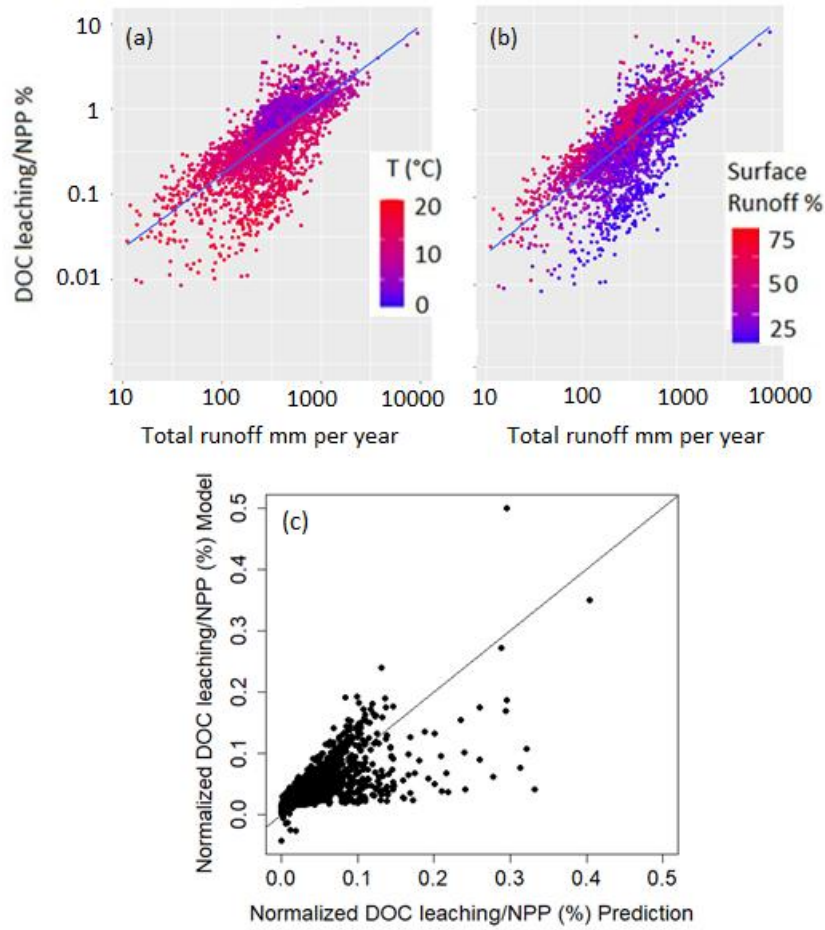
Figure 12. Simulated DOC leaching flux ($\text{gC m}^{-2} \text{ month}^{-1}$) (blue) and total runoff (mm per month) (red) for the six largest climate zones in Europe (period 2004-2006).

680 To further explore the environmental controls of the DOC leaching, we calculate the partial correlation factor for surface runoff, drainage, temperature and NPP and they are respectively 0.43, 0.54, -0.17 and 0.18, highlighting that surface runoff and drainage can explain most of the spatio-temporal variability in DOC leaching fluxes, temperature and NPP only playing a subordinate role. We decided to express DOC leaching as fraction of the annual terrestrial NPP (Figure 13). Doing this, we assume that NPP, which is undoubtedly the ultimate C source for DOC production (since litter and SOC stocks, the sources of DOC, are fed by NPP), is as well an important control of the DOC leaching flux. Moreover, normalizing DOC leaching by NPP, we strive to show the possible influence of other controls, allowing for a more in-depth analysis of the effect of hydrology and climate on the DOC leaching flux. Figure 13 reveals that the fraction of terrestrial NPP lost to DOC leaching increases, as expected, with total runoff. Moreover, this fraction increases with the contribution of surface runoff to total water loss from surface runoff plus drainage (Fig. 13b). This can be explained by the general decrease in soil DOC concentrations with depth (Fig. 6), leading to higher DOC concentrations in surface runoff than in drainage. In fact, according to our simulations, 97% of the leached DOC is concentrated in the surface runoff. Note that higher total runoff is often associated with a higher contribution of surface runoff, which leads to a ‘flushing effect’ where high runoff events contribute a disproportionate high fraction of the long-term DOC leaching (Idir et al. 1999, Raymond and Saiers 2010). Finally, we found higher leaching to NPP ratios at lower temperatures (Fig. 13a), suggesting that lower temperatures lead to longer turnover times of DOC in the soil, and thus higher concentrations in the leaching flux (section 2.1.2).

685

690

695



700 **Figure 13. Fraction (%) of terrestrial NPP that is leached as DOC in the river network as a function of total runoff. Each point represents the grid-cell average of both metrics for the entire simulation period (1979-2006). In panel (a) the color scale represents the grid-cell average temperature (°C) while in panel (b), the color scale represents the ratio of surface runoff to total runoff in percentage. Panel (c) shows the normalized predicted DOC leaching flux to NPP ratio (equation 13) against the normalized simulated values.**

To better quantify the effects of all these drivers on DOC leaching, we fitted a multi-linear regression model to predict the ratio of DOC leaching to NPP as a function of surface runoff, drainage and temperature at all grid points and for each month over the simulation period (eq. 13). The idea behind this rationale is to highlight that once normalized to the terrestrial NPP, we can directly analyse which physical drivers impact the fraction of NPP that is lost to leaching from terrestrial ecosystems. To compare the importance of each predictor for the spatiotemporal patterns of DOC leaching, we normalized all variables, V_i , of equation 13 according to equation 14 (where i is the cell index).

$$\frac{DOC\ leaching}{NPP} = K_0 + K_R * Runoff + K_D * Drainage + K_T * e^{T(^{\circ}C)} \quad (13)$$

$$K_0 = 0.01 \pm 7 * 10^{-4}$$

$$K_R = 0.342 \pm 0.009$$

$$K_D = 0.276 \pm 0.014$$

$$K_T = -0.055 \pm 0.013$$

710 (p-value < $2 * 10^{-16}$ except for temperature where p-value = $2.7 * 10^{-5}$)

$$V_{i,N} = \frac{V_i - V_{min}}{V_{max} - V_{min}} \quad (14)$$

To rule out any significant multi-collinearity in the regression model, we calculated for each predictor the Variance Inflation Factor (VIF). The VIF evaluates the correlations among all predictors which could impact the robustness of the regression

715 model (James et al., 2017). The closer the VIF is to 1, the more robust is the model. In our regression, VIF's of the runoff, drainage and temperature are respectively 1.13, 1.13 and 1.01, confirming that our prediction is robust and not biased by high multicollinearity.

In Fig. 13 (c), the DOC leaching simulated by ORCHILEAK is compared with the one predicted by equation 13. Our simple regression model is able to reproduce the simulations with a residual standard error of 0.68% and a R² of 0.45. The coefficients of our regression model reveal that spatio-temporal variability in DOC leaching is mainly driven by the surface runoff (K_R) and drainage (K_D). Air temperature as third control of DOC leaching is of subordinate importance as reflected by its low predictor's coefficient (K_T).

720 Table 4 summarizes, for each climate zone in Europe, the DOC leaching fluxes (in absolute value and normalized by the NPP) as well as other important components of the terrestrial C budget. Since runoff and temperature were identified as the controlling factors of the DOC leaching flux, normalized DOC leaching fluxes are expected to be significantly different among climate zones. Indeed, the fraction of NPP lost to the river network as DOC is the lowest in the semi-arid region (0.13%) where annual precipitation is low (total runoff around 92 mm per year) and temperatures are high.

Table 4. Key physical and biogeochemical characteristics of the six dominant climate zones of the European domain.

Variables	Unit	Semi-arid	Mediterranean	Oceanic	Humid continental	Subarctic	Tundra
Area	km ²	3.01E+11	8.74E+11	1.38E+12	2.11E+12	9.03E+11	1.56E+11
Leaching	gC m ⁻² yr ⁻¹	0.35	1.01	2.73	2.5	2.84	4.2
NPP		264.1	389.9	561.3	526.4	338.3	344.2
HR		175.5	278.6	390.6	345.7	255.3	266.9
Harvest (crop)		74.7	68	111.8	112.6	15.7	30.5
Harvest (wood)		5.4	25	46.1	40.7	41	41.8
LUC		-0.04	-4.8	-5.3	-7.7	-15.9	-3.7
NEE calculated		87	107.5	160	175	82.1	73.7
Leaching/NPP	%	0.13	0.26	0.49	0.48	0.84	1.22
Leaching/NEE		0.4	0.94	1.71	1.43	3.46	5.7
Runoff	Mm yr ⁻¹	30	63	82	91	236	404
Drainage		62	229	406	236	290	517
Temperature	°C	15	14.6	10.4	7.8	1.8	4.6

730 The highest fraction of NPP exported to rivers as DOC is found in the tundra climate and reach 1.22%. That can be explained by high runoff and drainage (reaching 920 mm per year) in this climate zone, but also by low temperatures lowering the fraction of DOC already decomposed within the soil column. The subarctic climate also presents a similarly high DOC leaching to NPP ratio with a value of 0.84%. The Mediterranean, Oceanic and humid continental climate zones present intermediate DOC leaching to NPP ratios of respectively 0.26%, 0.48% and 0.49%. Averaged over the whole of the EU-27, the DOC leaching flux normalized to the NPP amounts to 0.60 %.

3.2.2 Comparison with previous assessments of DOC leaching

In one of the first studies on the terrestrial C budget of Europe (Janssens et al., 2003) an imbalance (missing sink) between atmospheric CO₂ inversions and bottom-up C stock change accounting was partly attributed to the loss of carbon from land to rivers in the form of DOC of around 4 gC m⁻² yr⁻¹. Our results, 2.6 ± 2.5 gC m⁻² yr⁻¹, support this hypothesis although we suggest a DOC leaching rate slightly lower than this early study. Our lower value may come from the fact that we did not simulate peatlands and organic soils which are known hotspots of DOC leaching (Leifeld and Menichetti 2018), in particular in areas such as the northern UK and Scandinavia. Uncertainties in the processes included or omitted in the model could also explain some of the discrepancy. In terms of temporal variability, we found the highest DOC leaching in winter averaged over the continent (8.9 TgC in total for the six months of winter October to March) and the lowest in summer (5.4 TgC over the period April to September), consistent with the findings of Kindler et al. (2011). In terms of drivers of the DOC leaching fluxes, our results are in line with empirical findings by Gielen et al. (2011) that identified hydrology as the main driver of the inter- and intra-annual variability in DOC leaching. Similar conclusions have also been drawn by other empirical studies (Michalzik et al., 2001, Neff and Asner 2001, Worrall and Burt 2007).

750 It is also interesting to compare our results with recent global and regional model studies of DOC leaching in tropical and boreal ecosystems. For the Amazon and Congo basins, Hastie et al. (2019, 2021) found that 12 and 4 % of the NPP is exported each year to inland waters in the form of DOC and CO₂, respectively – much higher than the one we report for Europe (0.6%) but this value only accounts for DOC. Note that for these tropical lowland river basins extensive riparian wetlands are an important source of DOC, which are of minor importance in Europe. For the Lena river basin located in the boreal region, Bowring et al. (2020) found a DOC leaching of NPP ratio of about 1.5%. In our model assessment, this ratio reaches a very similar value of 1.2% for the boreal portion of Europe. For the temperate zone, a ratio of 0.35% for the East Coast of the US can be calculated when dividing the average DOC leaching flux of 2.7 gC m⁻² yr⁻¹ simulated by Tian et al. (2015) by the average NPP of 780 gC m⁻² yr⁻¹ estimated by Zhao et al. (2005). Further, our value is quite similar to the one extracted from the global study by Nakhavali et al. (2020) that amounts to 0.5 % for the European domain only. Overall, this comparison highlights that in Europe, the fraction of NPP lost as DOC to the river network is significantly smaller than in other regions of the world. The lower value is likely due to the lower connectivity between terrestrial and aquatic systems due to the lack of extensive wetlands, which have been reduced by major regulation of the European river network.

3.2.3 Implications for the terrestrial carbon budget of Europe

765 The terrestrial carbon budget is controlled by NPP, heterotrophic respiration, crop and wood harvesting and land use change. Here we look at the net ecosystem exchange (NEE) which is the net C exchange between land and atmosphere (Kramer et al., 2002). However, this view neglects the leakiness of terrestrial ecosystems that permanently removes a fraction of the land C and export it to the river network. Moreover, we can argue that DOC leaching represents a fraction of NEE, while the remainder of NEE can be attributed to harvest, land use change and changes in biomass and soil C stocks. From 1979 to 2012, the average NEE in Europe is 860 TgC yr⁻¹ (123 gC m⁻² yr⁻¹), equalling about 28% of the total NPP (Fig. 14b). The

ratio of DOC leaching to NEE shows drastic spatial variation, varying from an average value of 0.4% in the semi-arid region to a value of 5.7% in the tundra region. For the whole Europe, the DOC leaching is about 3% of the NEE.

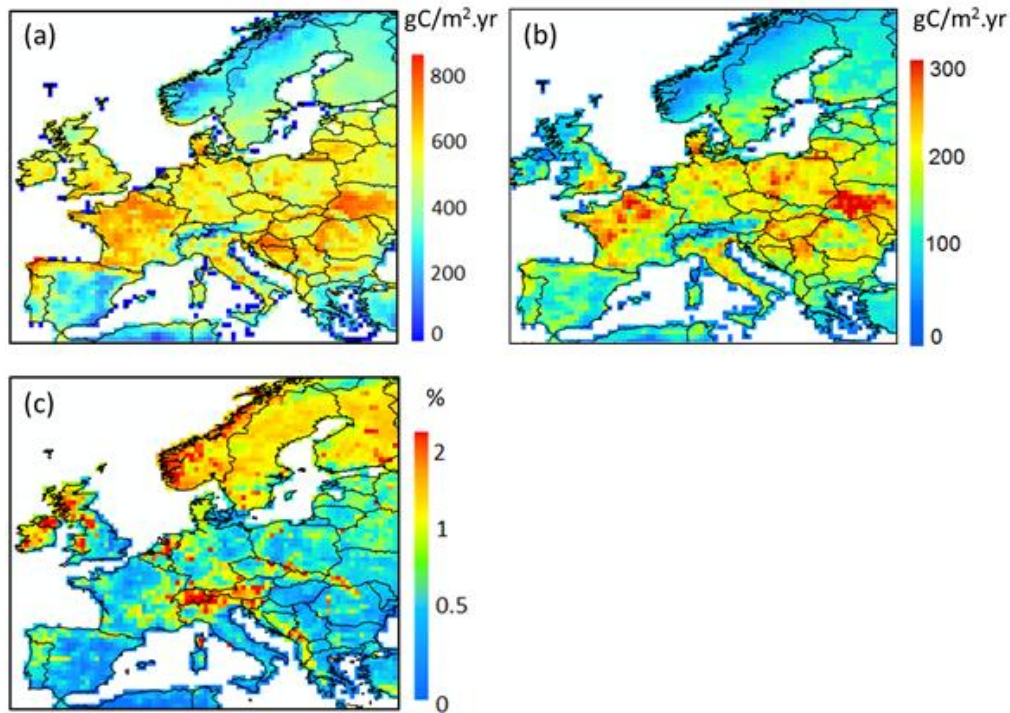


Figure 14. Grid-cell average of (a) Net Primary Production (NPP), (b) Net Ecosystem Exchange (NEE) and (c) fraction of NPP leached to the river network as DOC (%) for the period 1979-2006

775

3.3 Model limitations

ORCHILEAK is a LSM that simulates the impact of riverine DOC transfers on the terrestrial C budget, but it still suffers from several limitations. In fact, ORCHILEAK cannot represent all biogeochemical transformation processes affecting DOC in the soil column and the river network (Lauerwald et al., 2017). For instance, environmental controls such as soil pH and ionic strength have been demonstrated to have an impact on DOC solubility in soils (Monteith et al., 2007) and thus affect DOC leaching to streams. Unfortunately, these processes are not represented in our model, as there are still no reliable methods and forcing data to simulate the dynamics of soil pH and ionic strength in the soil solution at large scale.

780

As mentioned before, peatlands are not included in the model, yet they cover a large part of Northern Europe. Peatlands are known to play an important role in the C cycle, and are an important source of DOC to the river network. One of the major next steps would thus be to merge ORCHILEAK with ORCHIDEE-PEAT, a new branch of the land surface model ORCHIDEE simulating the development and C balance of peatlands (Qiu et al., 2019).

785

Another source of DOC originates from wastewater treatments plants that are not included in the model due to the lack of forcing data related to the sewage water treatment. It has been shown that DOC concentrations in sewage are important (Griffith et al 2009). However, Meybeck (1986) showed that DOC from sewage is very labile and only affects the concentration within short distances downstream of water processing plants. Having avoided observation data from sites known to be impacted by sewage effluents directly, we assume that our model-data evaluation was not impacted by this potential DOC source. For assessing the role of soil DOC leaching in the terrestrial C budget, sewage is not a contribution of direct interest.

790

While riparian zones are a major source of DOC to the river network (Inamdar and Mitchell 2006, Grabs et al. 2012), the impact of riparian zones on DOC leaching through runoff to the river network is only implicitly represented in the model (as described in Lauerwald et al. 2017). Due to the coarse resolution of the model, riparian zones around small streams (order 1 to 3) cannot be explicitly included in the model. It is assumed that the extent of the riparian zones, from which most of the

795

DOC stems, scales linearly to the surface area of these small streams, both in time as well as in space (i.e. between different grid cells of our model grid). While the surface area of these small streams is not directly represented, Lauerwald et al. (2017) assumed that spatial and temporal variations in this stream surface area scales to the square root of discharge that is flowing through these streams, roughly in line with empirical scaling laws (e.g. Raymond et al. 2012). For the larger rivers, for which the surface area is explicitly represented in the model, it is assumed that the inundated riparian zone can temporally make up to 10% of the river water surface area, depending on the temporal variability of discharge. Here, DOC produced from decomposition of litter and SOC is directly injected into the river water body.

ORCHILEAK could further be improved through the implementation of lakes and reservoirs. It has been shown that dams have a direct impact on C retention efficiency in the inland water river network (Maavara et al., 2017). So far, ORCHILEAK does not represent lateral transport of POC at continental scale, yet its non-negligible role in the terrestrial C budget has been demonstrated (Zhang et al. 2018; 2020, Naipal et al. 2019). Finally, the effect of nutrient limitation on the C cycle is not yet account for in ORCHILEAK. It has been demonstrated that the implementation of nitrogen (N) and phosphorus (P) could reduce the simulated land C sink (Goll et al. 2012, Sun et al. 2021). It can be assumed that nutrient limitation would similarly affect DOC leaching, and could dampen its increase with rising atmospheric CO₂ levels predicted by previous studies with ORCHILEAK (Lauerwald et al. 2020, Hastie et al. 2021).

4 Conclusion

We reconstructed the terrestrial and riverine C fluxes in Europe during the period 1979-2012 using the ORCHILEAK LSM. The total C leaching from soil to European rivers is 14.3 TgC yr⁻¹ on average, about 0.6 % of the estimated NPP and 3% of the terrestrial net up-take of atmospheric C. This flux shows large spatial and temporal variations. In specific, DOC leaching overall increases from warm and dry regions to cold and wet regions. However, since the model does not represent peatlands yet, the simulation results for subarctic and tundra regions in northern Europe could be biased. For the whole of Europe, DOC leaching rate is the highest in winter and lowest during the summer, mainly controlled by the seasonal variation of runoff. The implementation of manure lead to a significant increase in DOC leaching over the oceanic and humid continental region where croplands and grasslands are dominant. Our results contribute to a better assessment of the land-ocean C fluxes in Europe and to a better understanding of the effects of lateral C transfer on the terrestrial C budget. Combined with recent large-scale studies in tropical and boreal biomes as well as along the east coast of the US, an emergent view regarding the global role of DOC leaching on the terrestrial C balance and its underlying drivers is progressively emerging.

Code and data availability

The model code used in this study is available at DOI : 10.14768/75AC2F47-4691-46AF-9B12-B1A9629CBC56
All forcing data set are listed in table 1. Data of observed discharge used in this study are available from the Global Runoff Data Center (GRDC) at www.bafg.de/GRDC. Data of observed DOC concentrations in France are provided by eau de France at <http://www.data.eaufrance.fr/>.

Supplement

The supplement related to this article is available in the attached file (pdf).

Author contribution

CG, RL, PR, PC designed the study. CG performed calibration and evaluation of the model, ran the simulations, and wrote the initial manuscript. RL updated the model code of ORCHILEAK to improve representation of soil hydrology and DOC

840 cycling. HZ implemented the representation of manure impacts on soil DOC dynamics into the model code. All co-authors
contributed to interpretation of model results and improvement of the manuscript.

Competing interests

The authors declare that they have no conflict of interest.

845

Acknowledgements

RL, PC and BG acknowledge funding from the French state aid managed by the ANR under the "Investissements d'avenir"
programme [ANR-16-CONV-0003]. HZ, PR and RL acknowledge the 'Lateral-CNP' project (No. 34823748) supported by
the Fonds de la Recherche Scientifique –FNRS. CG and PR acknowledges funding from the European Union's Horizon 2020
850 research and innovation programme under Grant Agreements N° 776810 (project VERIFY) and N° 101003536 (ESM 2025).

References

- Abril G., M. Nogueira, H. Etcheber, G. Cabeçadas, E. Lemaire, M. Brogueira. Behaviour of organic carbon in nine
contrasting European estuaries. *Estuar. Coast. Shelf Sci.*, 54, pp. 241-262, 2002.
- 855 Avitabile, V., Camia, A.,. An assessment of forest biomass maps in Europe using harmonized national statistics and
inventory plots. *For. Ecol. Manage.* 409, 489–498, 2018
- Berggren, M. Al-Kharusi, E.S. Decreasing organic carbon bioreactivity in European rivers. *Freshw. Biol.*, 65 (6), pp. 1128-
1138, 10.1111/fwb.v65.610.1111/fwb.13498, 2020
- 860 Bloom, Anthony; Williams, Mathew. CARDAMOM 2001-2010 global carbon Model-Data Fusion (MDF) analysis, 2001-
2010 [dataset]. University of Edinburgh. School of GeoSciences. <https://doi.org/10.7488/ds/316>, 2015
- Bowring, S. P. K., Lauerwald, R., Guenet, B., Zhu, D., Guimberteau, M., Tootchi, A., Ducharne, A., and Ciais, P:
865 ORCHIDEE MICT-LEAK (r5459), a global model for the production, transport, and transformation of dissolved organic
carbon from Arctic permafrost regions – Part 1: Rationale, model description, and simulation protocol, *Geosci. Model Dev.*,
12, 3503–3521, <https://doi.org/10.5194/gmd-12-3503-2019>, 2019.
- Bowring, S. P. K., Lauerwald, R., Guenet, B., Zhu, D., Guimberteau, M., Regnier, P., Tootchi, A., Ducharne, A., and Ciais,
870 P.: ORCHIDEE MICT-LEAK (r5459), a global model for the production, transport, and transformation of dissolved organic
carbon from Arctic permafrost regions – Part 2: Model evaluation over the Lena River basin, *Geosci. Model Dev.*, 13, 507–
520, <https://doi.org/10.5194/gmd-13-507-2020>, 2020.
- Camino-Serrano, M., Gielen, B., Luyssaert, S., Ciais, P., Vicca, S., Guenet, B., Vos, B. De, Cools, N., Ahrens, B., Altaf
875 Arain, M., Borken, W., Clarke, N., Clarkson, B., Cummins, T., Don, A., Pannatier, E. G., Laudon, H., Moore, T., Niemi-
nen, T. M., Nilsson, M. B., Peichl, M., Schwendenmann, L., Siemens, J., and Janssens, I.: Linking variability in soil so-
lution dissolved organic carbon to climate, soil type, and vegetation type, *Global Biogeochem. Cy.*, 28, GB004726,
<https://doi.org/10.1002/2013gb004726>, 2014.

- 880 Camino-Serrano, M., Guenet, B., Luysaert, S., Ciais, P., Bastrikov, V., De Vos, B., Gielen, B., Gleixner, G., Jornet-Puig, A., Kaiser, K., Kothawala, D., Lauerwald, R., Peñuelas, J., Schrumph, M., Vicca, S., Vuichard, N., Walmsley, D., and Janssens, I. A.: ORCHIDEE-SOM: modeling soil organic carbon (SOC) and dissolved organic carbon (DOC) dynamics along vertical soil profiles in Europe, *Geosci. Model Dev.*, 11, 937–957, <https://doi.org/10.5194/gmd-11-937-2018>, 2018.
- 885 Campoy, A., Ducharne, A., Cheruy, F., Hourdin, F., Polcher, J., and Dupont, J. C.: Response of land surface fluxes and precipitation to different soil bottom hydrological conditions in a general circulation model, *J. Geophys. Res.-Atmos.*, 118, 10725–10739, <https://doi.org/10.1002/Jgrd.50627>, 2013.
- Ciais, P., et al. (2013), Carbon and other biogeochemical cycles, in *Climate Change: The Physical Science Basis. Contribution of Working Group I to the Fifth Assessment Report of the Intergovernmental Panel on Climate Change*, edited by T. F. Stocker et al., Cambridge Univ. Press, Cambridge, U. K., and New York, 2013.
- 890 Cole, J.J., Prairie, Y.T., Caraco, N.F., McDowell, W.H., Tranvik, L.J., Striegl, R.G., Duarte, C.M., Kortelainen, P., Downing, J.A., Middelburg, J.J., Melack, J.: Plumbing the global carbon cycle: integrating inland waters into the terrestrial carbon budget. *Ecosystems* 10 (1), 171–184, 2007.
- 895 Delpla I, Baures E, Jung AV, Thomas O. Impacts of rainfall events on runoff water quality in an agricultural environment in temperate areas. *Sci Total Environ.* 409(9): 1683–8. <https://doi.org/10.1016/j.scitotenv.2011.01.033>, 2011.
- 900 Drake, T. W., P. A. Raymond, and R. G. M. Spencer. Terrestrial carbon inputs to inland waters: a current synthesis of estimates and uncertainty. *Limnology and Oceanography Letters* 3:132–142. <http://doi.org/10.1002/lol2.1005>, 2018.
- FAO/IIASA/ISRIC/ISS-CAS/JRC. Harmonized World Soil Database (version 1.2). FAO, Rome, Italy and IIASA, Laxenburg, Austria, 2012
- 905 Farjalla VF, Marinho CC, Faria BM, Amado AM, Esteves FA, Bozelli RL, Giroldo D: Synergy of fresh and accumulated organic matter to bacterial growth. *Microb Ecol* 57(4):657–666. doi: 10.1007/s00248-008-9466-8, 2009.
- Fonte ES, Amado AM, Meirelles-Pereira F, Esteves FA, Rosado AS, Farjalla VF: The combination of different carbon sources enhances bacterial growth efficiency in aquatic ecosystems. *Microb Ecol* 66(4):871–878. doi:10.1007/s00248-013-0277-1, 2013.
- Fransner F, Nycander J, Mörth C-M et al: Tracing terrestrial DOC in the Baltic Sea—a 3-D model study. *Global Biogeochem Cycle* 30:134–148. doi:[10.1002/2014GB005078](https://doi.org/10.1002/2014GB005078), 2016.
- 915 Friedlingstein P., O’Sullivan M., Jones M.W., Andrew R.M., Hauck J., Olsen A., *et al.* Global carbon budget 2020. *Earth Syst Sci Data*, 12, pp. 3269-3340, [10.5194/essd-12-3269-2020](https://doi.org/10.5194/essd-12-3269-2020), 2020.
- Gielen, B., Neiryneck, J., Luysaert, S., and Janssens, I. A.: The importance of dissolved organic carbon fluxes for the carbon balance of a temperate Scots pine forest, *Agr. Forest Meteorol.*, 151, 270–278, <https://doi.org/10.1016/j.agrformet.2010.10.012>, 2011.

- 925 Goll, D. S., Brovkin, V., Parida, B. R., Reick, C. H., Kattge, J., Reich, P. B., van Bodegom, P. M., and Niinemets, Ü.: Nutrient limitation reduces land carbon uptake in simulations with a model of combined carbon, nitrogen and phosphorus cycling, *Biogeosciences*, 9, 3547–3569, <https://doi.org/10.5194/bg-9-3547-2012>, 2012.
- 930 Goll, D. S., Vuichard, N., Maignan, F., Jornet-Puig, A., Sardans, J., Violette, A., Peng, S., Sun, Y., Kvakic, M., Guimberteau, M., Guenet, B., Zaehle, S., Penuelas, J., Janssens, I., and Ciais, P.: A representation of the phosphorus cycle for ORCHIDEE (revision 4520), *Geosci. Model Dev.*, 10, 3745–3770, <https://doi.org/10.5194/gmd-10-3745-2017>, 2017.
- Goll, D. S., Joetzjer, E., Huang, M., and Ciais, P.: Low phosphorus availability decreases susceptibility of tropical primary productivity to droughts, *Geophys. Res. Lett.*, 45, 8231–8240, <https://doi.org/10.1029/2018GL077736>, 2018. Qiu, C., Zhu, D., Ciais, P., Guenet, B., Peng, S., Krinner, G., Tootchi, A., Ducharne, A., and Hastie, A.: Modelling northern peatland area and carbon dynamics since the Holocene with the ORCHIDEE-PEAT land surface model (SVN r5488), *Geosci. Model Dev.*, 12, 2961–2982, <https://doi.org/10.5194/gmd-12-2961-2019>, 2019.
- 935 Grabs, Thomas, et al. "Riparian zone hydrology and soil water total organic carbon (TOC): implications for spatial variability and upscaling of lateral riparian TOC exports." *Biogeosciences* 9.10: 3901-3916, 2012.
- Griffith, David R., Rebecca T. Barnes, and Peter A. Raymond. "Inputs of fossil carbon from wastewater treatment plants to US rivers and oceans." *Environmental Science & Technology* 43.15: 5647-5651, 2009.
- 940 Guimberteau, M., Drapeau, G., Ronchail, J., Sultan, B., Polcher, J., Martinez, J.-M., Prigent, C., Guyot, J.-L., Cochonneau, G., Espinoza, J. C., Filizola, N., Fraizy, P., Lavado, W., De Oliveira, E., Pombosa, R., Noriega, L., and Vauchel, P.: Discharge simulation in the sub-basins of the Amazon using ORCHIDEE forced by new datasets, *Hydrol. Earth Syst. Sci.*, 16, 911–935, <https://doi.org/10.5194/hess-16-911-2012>, 2012.
- 945 Guimberteau, M., Zhu, D., Maignan, F., Huang, Y., Yue, C., Dantec-Nédélec, S., Otlé, C., Jornet-Puig, A., Bastos, A., Laurent, P., Goll, D., Bowering, S., Chang, J., Guenet, B., Tifafi, M., Peng, S., Krinner, G., Ducharne, A., Wang, F., Wang, T., Wang, X., Wang, Y., Yin, Z., Lauerwald, R., Joetzjer, E., Qiu, C., Kim, H., and Ciais, P.: ORCHIDEE-MICT (v8.4.1), a land surface model for the high latitudes: model description and validation, *Geosci. Model Dev.*, 11, 121–163, <https://doi.org/10.5194/gmd-11-121-2018>, 2018.
- Hartmann, J., Lauerwald, R., and Moosdorf, N.: A brief overview of the GLObal RIVer CHEmistry Database, GLORICH, *Procedia, Earth Planet. Sci.*, 10, 23–27, 2014.
- 955 Hastie, A., Lauerwald, R., Ciais, P., Regnier, P. Aquatic carbon fluxes dampen the overall variation of net ecosystem productivity in the Amazon basin: An analysis of the interannual variability in the boundless carbon cycle. *Global Change Biology*, 25: 2094–2111. <https://doi.org/10.1111/gcb.14620>, 2019.
- 960 Hastie, A., Lauerwald, R., Ciais, P., Papa, F., and Regnier, P.: Historical and future contributions of inland waters to the Congo basin carbon balance, *Earth Syst. Dynam.*, 12, 37–62, <https://doi.org/10.5194/esd-12-37-2021>, 2021.
- Humbert, G., Parr, T.B., Jeanneau, L. et al. Agricultural Practices and Hydrologic Conditions Shape the Temporal Pattern of Soil and Stream Water Dissolved Organic Matter. *Ecosystems* 23, 1325–1343. <https://doi.org/10.1007/s10021-019-00471-w>, 2020

- 965 Idir, S., A.Probst, D.Viville, and J. L.Probst, Contribution of saturated areas and hillslopes to the water and element fluxes exported during a storm event: Tracing with dissolved organic carbon and silica. The Strengbach catchment case study (Vosges, France), *C. R. Acad. Sci., Ser. II*, **328**(2), 89–96, doi:[10.1016/s1251-8050\(99\)80003-2](https://doi.org/10.1016/s1251-8050(99)80003-2), 1999.
- Inamdar, Shreeram P., and Myron J. Mitchell. "Hydrologic and topographic controls on storm-event exports of dissolved organic carbon (DOC) and nitrate across catchment scales." *Water Resources Research* 42.3, 2006.
- 970 James, Gareth; Witten, Daniela; Hastie, Trevor; Tibshirani, Robert. *An Introduction to Statistical Learning* (8th ed.). Springer Science+Business Media New York. [ISBN 978-1-4614-7138-7](https://doi.org/10.1007/978-1-4614-7138-7), 2017.
- Janssens, I. A., Freibauer, A., Ciais, P., Smith, P., Nabuurs, G. J., Folberth, G., Schlamadinger, B., Hutjes, R. W. A.,
975 Ceulemans, R., Schulze, E. D., Valentini, R., and Dolman, A. J.: Europe's terrestrial biosphere absorbs 7 to 12% of european anthropogenic CO₂ emissions, *Science*, 300, 1538–1542, 2003
- Kalbitz, K., Schmerwitz, J., Schwesig, D., and Matzner, E.: Biodegradation of soil-derived dissolved organic matter as related to its properties, *Geoderma*, 113, 273–291, 2003.
- 980 Kicklighter DW, et al. Insights and issues with simulating terrestrial DOC loading of Arctic river networks. *Ecol Appl* 23(8):1817–1836, 2013.
- Kindler, R., Siemens, J., Kaiser, K., Walmsley, D. C., Bernhofer, C., Buchmann, N., Cellier, P., Eugster, W., Gleixner, G.,
985 Grunwald, T., Heim, A., Ibrom, A., Jones, S. K., Jones, M., Klumpp, K., Kutsch, W., Larsen, K. S., Lehuger, S., Loubet, B., Mckenzie, R., Moors, E., Osborne, B., Pilegaard, K., Rebmann, C., Saunders, M., Schmidt, M. W. I., Schruppf, M., Seyfferth, J., Skiba, U., Soussana, J.-F., Sutton, M. A., Tefs, C., Vowinckel, B., Zeeman, M. J., and Kaupenjohann, M. Dissolved carbon leaching from soil is a crucial component of the net ecosystem carbon balance, *Glob. Change Biol.*, 17, 1167–1185, <https://doi.org/10.1111/j.1365-486.2010.02282.x>, 2011.
- 990 Köchy, M., Hiederer, R., & Freibauer, a. Global distribution of soil organic carbon – Part 1: Masses and frequency distributions of SOC stocks for the tropics, permafrost regions, wetlands, and the world. *Soil*, 1(1), 351–365. <https://doi.org/10.5194/soil-1-351-2015>, 2015.
- 995 Kramer K, Leinonen I, Bartelink HH et al. Evaluation of six process-based forest growth models using eddy-covariance measurements of CO₂ and H₂O fluxes at six forest sites in Europe. *Global Change Biology*, 8, 213–230, 2002.
- Krinner, G. et al. A dynamic global vegetation model for studies of the coupled atmosphere-biosphere system. *Global Biogeochem. Cycles* 19, 1–33, 2005.
- 1000 Lauerwald, R., Hartmann, J., Ludwig, W. & Moosdorf, N. Assessing the nonconservative fluvial fluxes of dissolved organic carbon in North America. *J. Geophys. Res.* **117**, G01027, 2012.
- Lauerwald, R., Laruelle, G. G., Hartmann, J., Ciais, P., & Regnier, P. A. G. Spatial patterns in CO₂ evasion from the global
1005 river network. *Global Biogeochemical Cycles*, 29(5), 534–554. <https://doi.org/10.1002/2014GB004941>, 2015

- Lauerwald, R., Regnier, P., Camino-Serrano, M., Guenet, B., Guimberteau, M., Ducharne, A., ... Ciais, P. ORCHILEAK (revision 3875): a new model branch to simulate carbon transfers along the terrestrial–aquatic continuum of the Amazon basin. *Geoscientific Model Development*, 10(10), 3821–3859. <https://doi.org/10.5194/gmd-10-3821-2017>, 2017.
- 1010
- Lauerwald, R., Regnier, P., Guenet, B., Friedlingstein, P., Ciais, P. How simulations of the land carbon sink are biased by ignoring fluvial carbon transfers –A case study for the Amazon basin, [Volume 3, Issue 2](#), 21 August 2020, Pages 226-236 <https://doi.org/10.1016/j.oneear.2020.07.009>, 2020
- 1015
- Lehner B, Verdin K, Jarvis A. New global hydrography derived from spaceborne elevation data. *EOS, Transactions of the American Geophysical Union* **89**: 93– 104, 2008.
- Leifeld, J., & Menichetti, L. The underappreciated potential of peatlands in global climate change mitigation strategies /704/47/4113 /704/106/47 article. *Nature Communications*, 9(1). <https://doi.org/10.1038/s41467-018-03406-6>, 2018.
- 1020
- Le Quéré, C., Moriarty, R., Andrew, R. M., Peters, G. P., Ciais, P., Friedlingstein, P., Jones, S. D., Sitch, S., Tans, P., Arneeth, A., Boden, T. A., Bopp, L., Bozec, Y., Canadell, J. G., Chini, L. P., Chevallier, F., Cosca, C. E., Harris, I., Hoppema, M., Houghton, R. A., House, J. I., Jain, A. K., Johannessen, T., Kato, E., Keeling, R. F., Kitidis, V., Klein Goldewijk, K., Koven, C., Landa, C. S., Landschützer, P., Lenton, A., Lima, I. D., Marland, G., Mathis, J. T., Metz, N., Nojiri, Y., Olsen, A., Ono, T., Peng, S., Peters, W., Pfeil, B., Poulter, B., Raupach, M. R., Regnier, P., Rödenbeck, C., Saito, S., Salisbury, J. E., Schuster, U., Schwinger, J., Séférian, R., Segschneider, J., Steinhoff, T., Stocker, B. D., Sutton, A. J., Takahashi, T., Tilbrook, B., van der Werf, G. R., Viovy, N., Wang, Y.-P., Wanninkhof, R., Wiltshire, A., and Zeng, N.: Global carbon budget 2014, *Earth Syst. Sci. Data*, 7, 47–85, <https://doi.org/10.5194/essd-7-47-2015>, 2015.
- 1025
- 1030
- Le Quéré, C., Andrew, R. M., Friedlingstein, P., Sitch, S., Pongratz, J., Manning, A. C., Korsbakken, J. I., Peters, G. P., Canadell, J. G., Jackson, R. B., Boden, T. A., Tans, P. P., Andrews, O. D., Arora, V. K., Bakker, D. C. E., Barbero, L., Becker, M., Betts, R. A., Bopp, L., Chevallier, F., Chini, L. P., Ciais, P., Cosca, C. E., Cross, J., Currie, K., Gasser, T., Harris, I., Hauck, J., Haverd, V., Houghton, R. A., Hunt, C. W., Hurtt, G., Ilyina, T., Jain, A. K., Kato, E., Kautz, M., Keeling, R. F., Klein Goldewijk, K., Körtzinger, A., Landschützer, P., Lefèvre, N., Lenton, A., Lienert, S., Lima, I.,
- 1035
- Lombardozi, D., Metz, N., Millero, F., Monteiro, P. M. S., Munro, D. R., Nabel, J. E. M. S., Nakaoka, S., Nojiri, Y., Padin, X. A., Peregón, A., Pfeil, B., Pierrot, D., Poulter, B., Rehder, G., Reimer, J., Rödenbeck, C., Schwinger, J., Séférian, R., Skjelvan, I., Stocker, B. D., Tian, H., Tilbrook, B., Tubiello, F. N., van der Laan-Luijckx, I. T., van der Werf, G. R., van Heuven, S., Viovy, N., Vuichard, N., Walker, A. P., Watson, A. J., Wiltshire, A. J., Zaehle, S., and Zhu, D.: Global Carbon Budget 2017, *Earth Syst. Sci. Data*, 10, 405–448, <https://doi.org/10.5194/essd-10-405-2018>, 2018.
- 1040
- Li, M., Peng, C., Zhou, X., Yang, Y., Guo, Y., Shi, G., & Zhu, Q. Modeling global riverine DOC flux dynamics from 1951 to 2015. *Journal of Advances in Modeling Earth Systems*, 11, 514–530. <https://doi.org/10.1002/2018MS001363>, 2019.
- Maavara, T., Lauerwald, R., Regnier, P., & Van Cappellen, P. Global perturbation of organic carbon cycling by river
- 1045
- damming. *Nature Communications*, 8(May), 1–10. <https://doi.org/10.1038/ncomms15347>, 2017
- Mattsson T., P. Kortelainen, A. Laubel, D. Evans, M. Pujo-Pay, A. Raeike, P. Conan. Export of dissolved organic matter in relation to land use along a European climatic gradient. *Sci. Total Environ.*, 407, pp. 1967-1976, 2009.

- 1050 Meybeck, M. Riverine transport of atmospheric carbon: sources, global typology and budget. *Water, Air and Soil Pollution* 70, 443–463, 1993a
- Meybeck, M. C, N, P and S in rivers: from sources to global inputs. In *Interactions of C, N, P and S Biogeochemical cycles and global change* (Wollast, R., Mackenzie, F. T. & Chou, L., eds). NATO ASI Series, 14. Springer-Verlag, Berlin, pp. 163–
- 1055 191, 1993b.
- Michalzik B., Kalbitz K., Park J.H. and Matzner E. Fluxes and concentrations of dissolved organic carbon and nitrogen – a synthesis for temperate forests. *Biogeochemistry* 52: 173–205, 2001.
- 1060 Moore, T. R., de Souza, W., and Koprivnjak, J.-F.: Controls on the sorption of dissolved organic carbon by soils, *Soil Sci.*, 154, 120– 129, 1992.
- Muñoz-Sabater J., Dutra, E., Agustí-Panareda, A., Albergel, C., Arduini, G., Balsamo, G., Boussetta, S., Choulga, M., Harrigan, S., Hersbach, H., Martens, B., Miralles, D. G., Piles, M., Rodríguez-Fernández, N. J., Zsoter, E., Buontempo, C.,
- 1065 and Thépaut, J.-N.: ERA5-Land: A state-of-the-art global reanalysis dataset for land applications, *Earth Syst. Sci. Data*, 13, 4349–4383, <https://doi.org/10.5194/essd-13-4349-2021>, 2021.
- Nakhavali, M., Friedlingstein, P., Lauerwald, R., Tang, J., Chadburn, S., Camino-Serrano, M., Guenet, B., Harper, A., Walmsley, D., Peichl, M., and Gielen, B.: Representation of dissolved organic carbon in the JULES land surface model (vn4.4_JULES-DOCM), *Geosci. Model Dev.*, 11, 593–609, <https://doi.org/10.5194/gmd-11-593-2018>, 2018.
- 1070 Nakhavali, M., Lauerwald, R., Regnier, P., Guenet, B., Chadburn, S., & Friedlingstein, P. Leaching of dissolved organic carbon from mineral soils plays a significant role in the terrestrial carbon balance, (June 2020), 1083–1096. <https://doi.org/10.1111/gcb.15460>, 2021
- 1075 Nash, J. E. and Sutcliffe, J. V.: River flow forecasting through conceptual models, Part I - A discussion of principles, *J. Hydrol.*, 10, 282–290, 1970.
- Neff J.C. and Asner G.P. Dissolved organic carbon in terrestrial ecosystems: a synthesis and a model. *Ecosystems* 4: 29–48, 2001.
- 1080 d'Orgeval, T., Polcher, J., & de Rosnay, P. Sensitivity of the West African hydrological cycle in ORCHIDEE to infiltration processes. *Hydrology and Earth System Sciences*, 12, 1387– 1401. <https://doi.org/10.5194/hess-12-1387-2008>, 2008.
- Parton, W. J., Stewart, J. W., and Cole, C. V.: Dynamics of C, N, P and S in grassland soils: a model, *Biogeochemistry*, 5,
- 1085 109–131, <https://doi.org/10.1007/bf02180320>, 1988.
- Peel, M. C., Finlayson, B. L., & McMahon, T. A. Updated world map of the Köppen-Geiger climate classification. *Hydrology and earth system sciences*, 11(5), 1633-1644, 2007.
- 1090 Peng, S., Ciais, P., Maignan, F., Li, W., Chang, J., Wang, T., and Yue, C.: Sensitivity of land use change emission estimates to historical land use and land cover mapping, *Global Biogeochem. Cy.*, 31, 626–643, <https://doi.org/10.1002/2015GB005360>, 2017.

- 1095 Polcher, J.: Les processus de surface à l'échelle globale et leurs interactions avec l'atmosphère, Habilitation à diriger des recherches, University Pierre et Marie Curie, Paris, France, 2003.
- Raymond PA, Saiers JE. Event controlled DOC export from forested watersheds. *Biogeochemistry* 100(1–3):197–209, 2010.
- 1100 Raymond, Peter A., et al. "Scaling the gas transfer velocity and hydraulic geometry in streams and small rivers." *Limnology and Oceanography: Fluids and Environments* 2.1: 41-53, 2012.
- Regnier, P., Friedlingstein, P., Ciais, P., Mackenzie, F. T., Gruber, N., Janssens, I. A., Laruelle, G. G., Lauerwald, R., Luysaert, S., Andersson, A. J., Arndt, S., Arnosti, C., Borges, A. V., Dale, A. W., Gallego-Sala, A., Goddérís, Y., Goossens, N., Hartmann, J., Heinze, C., Ilyina, T., Joos, F., Larowe, D. E., Leifeld, J., Meysman, F. J. R., Munhoven, G., Raymond, P. A., Spahni, R., Suntharalingam, P., and Thullner, M.: Anthropogenic perturbation of the carbon fluxes from land to ocean, *Nat. Geosci.*, 6, 597–607, <https://doi.org/10.1038/ngeo1830>, 2013.
- 1105 Reynolds, C., Jackson, T. & Rawls, W. Estimating available water content by linking the FAO soil map of the world with global soil profile databases and pedo-transfer functions. *Am. Geophys. Union Fall Meet. EOS Trans. Spring Meet. Suppl.* 80, S132 426, 1999.
- 1110 de Rosnay, P., Polcher, J., Bruen, M., and Laval, K.: Impact of a physically based soil water flow and soil-plant interaction representation for modeling large-scale land surface processes, *J. Geophys. Res.-Atmos.*, 107, 4118, <https://doi.org/10.1029/2001JD000634>, 2002.
- 1115 Royer, I.; Angers, D. A.; Chantigny, M. H.; Simard, R. R.; Cluis, D. Dissolved organic carbon in runoff and tile-drain water under corn and forage fertilized with hog manure. *J. Environ. Qual.* 2007, 36, 855–863. doi: 10.2134/jeq2006.0355, 2006.
- 1120 Saxton KE, Rawls WJ, Romberger SJ, Papendick RI. Estimating generalized soil-water characteristics from texture. *Soil Science Society of America Journal*, 50, 1031–1036, 1986.
- Singh, S., Dutta, S., and Inamdar, S.: Land application of poultry manure and its influence on spectrofluorometric characteristics of dissolved organic matter, *Agriculture, Ecosystems and Environment*, 193, 25–36, <https://doi.org/10.1016/j.agee.2014.04.019>, 2014. Zhang, H., Goll, D. S., Manzoni, S., Ciais, P., Guenet, B., and Huang, Y.: Modeling the effects of litter stoichiometry and soil mineral N availability on soil organic matter formation using CENTURY-CUE (v1.0), *Geosci. Model Dev.*, 11, 4779–4796, <https://doi.org/10.5194/gmd-11-4779-2018>, 2018.
- 1125 Sitch, S. et al., Evaluation of ecosystem dynamics, plant geography and terrestrial carbon cycling in the LPJ dynamic global vegetation model, *Glob. Chang. Biol.*, 9(2), 161–185, doi:10.1046/j.1365-2486.2003.00569.x, 2003.
- 1130 Smith, J., Gottschalk, P., Bellarby, J., Chapman, S., Lilly, A., Towers, W., Bell, J., Coleman, K., Nayak, D., Richards, M., Hillier, J., Flynn, H., Wattenbach, M., Aitkenhead, M., Yeluripurti, J., Farmer, J., Milne, R., Thomson, A., Evans, C., and Smith, P.: Estimating changes in national soil carbon stocks using ECOSSE – a new model that includes upland organic soils. Part II. Application in Scotland, *Clim. Res.*, 45, 193–205, <https://doi.org/10.3354/cr00902>, 2010.
- 1135

- Sun, Y., Goll, D. S., Chang, J., Ciais, P., Guenet, B., Helfenstein, J., Huang, Y., Lauerwald, R., Maignan, F., Naipal, V., Wang, Y., Yang, H., and Zhang, H.: Global evaluation of the nutrient-enabled version of the land surface model ORCHIDEE-CNP v1.2 (r5986), *Geosci. Model Dev.*, 14, 1987–2010, <https://doi.org/10.5194/gmd-14-1987-2021>, 2021.
- 1140 Tian, H., Q. Yang, R. G. Najjar, W. Ren, M. A. M. Friedrichs, C. S. Hopkinson, and S. Pan: Anthropogenic and climatic influences on carbon fluxes from eastern North America to the Atlantic Ocean: A process-based modeling study, *J. Geophys. Res. Biogeosci.*, 120, 752–772, doi:10.1002/2014JG002760, 2015.
- Turgeon, J.: Production and biodegradation of dissolved carbon, nitrogen and phosphorus from Canadian forest floors, 1145 McGill University, 2008.
- Turner D.P., W.D. Ritts, W.B. Cohen, S.T. Gower, S.W. Running, M. Zhao, M.H. Costa, A.A. Kirschbaum, J.M. Ham, S.R. Saleska, D.E. Ahl. Evaluation of MODIS NPP and GPP products across multiple biomes. *Remote Sens. Environ.*, 102 (3-4), pp. 282-292, [10.1016/j.rse.2006.02.017](https://doi.org/10.1016/j.rse.2006.02.017), 2006.
- 1150 Vorosmarty, C. J., B. M. Fekete, M. Meybeck, and R. B. Lammers, Geo- morphometric attributes of the global system of rivers at 30-minute spa- tial resolution, *J. Hydrol.*, 237, 17–39, 2000.
- Vuichard et al., Accounting for Carbon and Nitrogen interactions in the Global Terrestrial Ecosystem Model ORCHIDEE 1155 (trunk version, rev 4999): multi-scale evaluation of gross primary production. *Geosci. Model Dev. Discuss.*, <https://doi.org/10.5194/gmd-2018-261>, 2018
- Wang, T., Otle, C., Boone, A., Ciais, P., Brun, E., Morin, S., ... & Peng, S. Evaluation of an improved intermediate complexity snow scheme in the ORCHIDEE land surface model. *Journal of Geophysical Research: Atmospheres*, 118(12), 1160 6064-6079, 2013.
- Weedon, G. P., G. Balsamo, N. Bellouin, S. Gomes, M. J. Best, and P. Viterbo, The WFDEI meteorological forcing data set: WATCH Forcing Data methodology applied to ERA-Interim reanalysis data, *Water Resour. Res.*, 50, 7505–7514, doi:10.1002/2014WR015638, 2014.
- 1165 Worrall, F., and T. P. Burt. Flux of dissolved organic carbon from U.K. rivers, *Global Biogeochem. Cycles*, 21, GB1013, doi:10.1029/2006GB002709, 2007.
- Worrall F. , Davies H., Bhogal A., Lilly A., Evans M.G. , Turner K., Burt T.P., Barraclough D. , Smith P. , Merrington 1170 G. The flux of DOC from the UK – predicting the role of soils, land use and in-stream losses. *J. Hydrol.*, 448–449, pp. 149-160, 2012.
- Yao, Y., Ciais, P., Viovy, N., Li, W., Cresto-Aleina, F., Yang, H., et al. A data-driven global soil heterotrophic respiration dataset and the drivers of its inter-annual variability. *Global Biogeochemical Cycles*, 35, 2020 GB006918. 1175 <https://doi.org/10.1029/2020GB006918>, 2021.

Zhang, B., Tian, H., Lu, C., Dangal, S. R. S., Yang, J., and Pan, S.: Global manure nitrogen production and application in cropland during 1860–2014: a 5 arcmin gridded global dataset for Earth system modeling, *Earth Syst. Sci. Data*, 9, 667–678, <https://doi.org/10.5194/essd-9-667-2017>, 2017.

1180

Zhang, H., Lauerwald, R., Regnier, P., Ciais, P., Yuan, W., Naipal, V., ... & Camino-Serrano, M. Simulating erosion-induced soil and carbon delivery from uplands to rivers in a global land surface model. *Journal of advances in modeling earth systems*, 12(11), e2020MS002121, 2020.

1185 Zhao, M., F. A. Heinsch, R. R. Nemani, and S. W. Running, Improvements of the MODIS terrestrial gross and net primary production global data set, *Remote Sens. Environ.*, 95(2), 164–176, doi:10.1016/j.rse.2004.12.011, 2005.